

AD 662726

RESEARCH ON COMBUSTION OF SOLID PROPELLANTS

TECHNICAL SUMMARY REPORT
COVERING THE PERIOD
1 JULY 1966 THROUGH 31 AUGUST 1967

CONTRACT NO.
DA-04-200-AMC-968(X)

D D C
REGISTERED
DEC 18 1968
RECEIVED
A

Prepared for

U.S. ARMY BALLISTICS RESEARCH LABORATORIES
ABERDEEN PROVING GROUND, MARYLAND

This document has been approved for public release and sale;
its distribution is unlimited.



United Technology Center

DIVISION OF UNITED AIRCRAFT CORPORATION
U
A

Available from the
CLEARINGHOUSE
for Federal Scientific & Technical
Information Springfield, Va. 22151

85

DISCLAIMER NOTICE

THIS DOCUMENT IS BEST QUALITY PRACTICABLE. THE COPY FURNISHED TO DTIC CONTAINED A SIGNIFICANT NUMBER OF PAGES WHICH DO NOT REPRODUCE LEGIBLY.

UTC 2136-TSR2
11 October 1967

RESEARCH ON COMBUSTION OF SOLID PROPELLANTS

Research and Advanced Technology Department
UNITED TECHNOLOGY CENTER
Division of United Aircraft Corporation
Sunnyvale, California

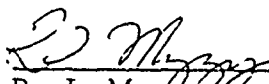
TECHNICAL SUMMARY REPORT
FOR THE PERIOD 1 JULY 1966 THROUGH 31 AUGUST 1967

Prepared for

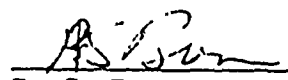
U. S. Army Ballistic Research Laboratories
Aberdeen Proving Ground, Maryland

Contract No. DA-04-200-AMC-968(x)

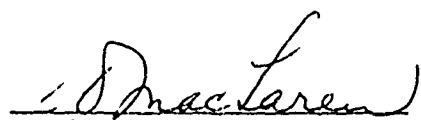
Prepared by:


R. J. Muzzy
Project Scientist

Submitted by:


R. S. Brown
Project Manager

Approved by:


R. O. MacLaren
Manager
Propulsion Research Branch

ABSTRACT

Experimental and theoretical studies have continued to evaluate the effects of surface reactions on the acoustic response function of composite solid propellants. Using a carboxy-terminated polybutadiene-ammonium perchlorate propellant, the effects of various coatings on the oxidizer crystals were investigated using a T-burner over a range of frequencies from 150 to 5,000 cps. The results show that coatings of Kel-F and Viton reduce the acoustic response, the reduction increasing with increasing coating level. The effect results from the coating on the oxidizer because incorporating the same quantity of coating material in the binder had no effect on the maximum response.

The influence of both chemical structure of the binder and curing agent was also investigated using CTPB, PBAA/AN, and UTREZ binders, and MAPO and epoxy curing systems. The data show PBAA/AN propellants have approximately 50% of the acoustical response of the CTPB propellants. On the other hand, the cure agent was responsible for greatest shift in the frequency at which the maximum admittance occurs. The mechanism responsible for this frequency shift currently is not understood.

Studies were made of the effects of pressure on a carboxy-terminated polybutadiene-ammonium perchlorate propellant. The results indicate that over a pressure range from 100 to 500 psia, both the maximum value of the acoustic response function and the frequency at which it occurs increase with increasing pressure.

Theoretical studies were conducted using a simplified combustion model which incorporates the effects of pressure-dependent surface reactions, pressure dependent gas phase reactions, heat transfer and surface pyrolysis reactions. Using a perturbation approach, the predicted acoustic admittance-frequency relation is characterized by three independent parameters. Parametric studies reveal that high ratios of the maximum acoustic response function to the burning rate pressure exponent are predicted when the net heat release at the propellant surface (pressure-dependent reactions plus pyrolysis reactions) is nearly zero or is exothermic. The stability of the combustion process in self-excited modes has also been considered theoretically and the stability bounds determined as a function of combustion parameters. The perturbation technique was expanded to examine the nonlinear behavior of the combustion model. Preliminary observations indicate that the effect of oscillating pressure on the burning rate changes is small and can be neglected.

CONTENTS

<u>Section</u>		<u>Page</u>
1.0	INTRODUCTION	1
2.0	TECHNICAL DISCUSSIONS	2
2.1	Experimental Studies	3
	2.1.1 Experimental Apparatus	3
	2.1.2 Propellant Formulations	4
	2.1.3 Experimental Results	4
	2.1.4 Photographic Studies	11
2.2	Theoretical Studies	21
	2.2.1 Analytical Combustion Model	21
	2.2.2 Linear Response Studies	24
	2.2.3 Comparison of Experiment and Theory in the Linear Region	31
	2.2.4 Nonlinear Response Studies	35
	REFERENCES	42
	APPENDIX A: Experimental Data	45
	APPENDIX B: Theoretical Analysis of Subsurface Reactions and Nonlinear Effects Using Finite Difference Techniques	71

ILLUSTRATIONS

<u>Figure</u>		<u>Page</u>
1	Effect of Kel-F and Viton Coatings on Acoustical Response	7
2	Effect of PBAN Binders	9
3	Response Functions for UTX-9173	10
4	Effect of Pressure on Acoustic Response	12
5	Effect of Pressure on Acoustic Response	13
6	NOTS A-13 Propellant Data	14
7	Acoustic Response of CTPB and UTREZ Binders	15
8	Schematic of Viewing Section	17
9	Photograph of Viewing Section	18
10	Camera Arrangement for Viewing Section	19
11	Photograph of Combustion Process in T-Burner Viewing Section	20
12	Stability Map for Self-Excited Modes	27
13	General Response of Linear Model	29
14	Acoustic Response Function - Moderate Surface Reaction Term Effect on Pressure	32
15	Predicted Acoustic Response of $n' \approx 0.5$ as a Function of λ'	
16	Predicted Acoustic Response for $n' = 1.0$ as a Function of λ'	34
17	Effect of D on Predicted Shift in Burning Rate	40
18	Effect of Pressure on Predicted Shift in Burning Rate	41

TABLES

<u>Table</u>		<u>Page</u>
I	Propellant Formulations Used to Test Coating Effect	5

Nomenclature

- $a^1 = 4 \alpha \omega^1 / r_o^2$
 $a_1 = 1 + a^1$
 $A^1 = M_i (1 + 2M_r)$
 $B^1 = M_r^2 - M_i^2 + M_r$
 $c =$ sonic velocity of the combustion gases
 $E^1 = M_r + 4SM_i/\lambda$
 $E_1 =$ activation energy of exothermic surface reactions
 $E_2 =$ activation energy of overall pyrolysis rate at surface
 $E_3 =$ activation energy of solid phase combustion reactions
 $E_f =$ activation energy of gas phase reactions
 $f_g, f_d =$ frequency of the acoustic pressure oscillations at the point where α_g and α_d measured
 $F_o =$ steady-state heat flux from gas phase combustion zone to solid surface
 $F =$ instantaneous heat flux from gas phase combustion zone to solid surface
 $\text{Im}(\mu/\epsilon) =$ imaginary part of acoustic response function
 $k =$ thermal conductivity
 $L =$ length of combustion chamber
 $M_1 = -1/2 [1 + \sqrt{1+s}]$
 $m^1 =$ order of gas phase reaction
 $M_i = -\left[(1+\lambda^2)^{1/4} \sin \nu \right] / 2$
 $M_r = -\left[1 + (1+\lambda^2)^{1/4} \cos \nu \right] / 2$

n = steady-state burning rate exponent

n^1 = pressure exponent on gas phase heat flux

\tilde{P} = instantaneous pressure

P_0 = steady-state pressure

P = amplitude of the acoustic pressure oscillation

\dot{r} = instantaneous linear burning rate of propellant

\dot{r}_0 = steady-state linear burning rate of propellant

$R = \frac{\beta - \Gamma\lambda}{\psi}$

$\text{Re}(\mu/\epsilon)$ = real part of acoustic response function

s = La Placian variable

$S = \frac{1-\theta}{\psi}$

t = time

T = temperature

T^0 = steady state temperature

T_f = propellant flame temperature

T_∞ = initial temperature of the propellant

x = distance into the solid from the surface

Z_1 = Arrhenius pre-exponential factor for exothermic surface reactions

Z_2 = Arrhenius pre-exponential factor for overall pyrolysis rate at surface

Z_3 = Arrhenius pre-exponential factor solid phase combustion reactions

Greek Symbols

- α = propellant thermal diffusivity
 α_d = dP_c/dt during the decay of the acoustic pressure oscillations
 α_g = dP_c/dt during the growth of the acoustic pressure oscillations
 β = $\Delta H_v / C_p T^\circ(0)$
 Γ = $P_o Z \exp(-E_1 \Delta RT^\circ(0)) / \dot{r}_o \rho C_p T(0)$
 ΔH_v = effective heat of gasification of propellant at the surface
 ϵ' = perturbation variable
 ϵ_1 = amplitude of the first harmonic pressure oscillations
 ϵ_2 = amplitude of second order pressure oscillations
 $\tilde{\epsilon}_2$ = instantaneous value of ϵ_1
 ζ = $\frac{\dot{r}_o x}{\alpha}$
 η = $F_o / r_o C_p T^\circ(0)$
 θ_1 = component of temperature oscillating with first harmonic
 θ_2 = component of temperature oscillating with second harmonic
 θ_2° = steady state state shift in temperature resulting from second
 t_2 = amplitude of second harmonic temperature oscillations resulting from second
 λ = E_1 / E_2
 λ = $4\alpha \omega / \dot{r}_o^2$
 λ' = $4\alpha \omega / Z_2^2$
 $\tilde{\mu}$ = first harmonic amplitude of μ
 μ_o = first harmonic oscillating component of burning rate
 $(E_2 \theta(0, \tau) / RT^{\circ 2}(0))$
 μ_2° = $\theta_2^\circ(0) / T^\circ(0) \psi$

Greek Symbols

- ρ = propellant density
- τ = dimensionless time $i_0 t / 4\alpha$
- ϕ = $T_\infty / T^\circ(0)$
- ψ = $RT^\circ(0) / E_2$
- ω = $2\pi f_g$
- ω' = complex frequency = $(\alpha_g + 2i\pi f_g)$
- ν = $0.5 \tan^{-1}(\lambda)$

1.0 INTRODUCTION

Unstable combustion of solid rocket propellants is of interest for two reasons: first, it is one of several methods available for investigating the structure of the solid propellant combustion and, second, unstable combustion has presented serious problems in the development of some operational solid propellant rocket motors. For these reasons, UTC has been investigating certain aspects of this problem, namely, pressure-coupled combustion instability, under Contract No. DA-04-200-AMC-968(X). The principal objective of these studies is to examine the relation between combustion instability as observed by pressure oscillations in the gas phase and exothermic reactions occurring on and within the solid phase surface.

Experimental studies have been directed toward investigating the effects of coatings on the solid oxidizer crystals; effects of the chemical and physical nature of the propellant binder, catalysts, and cross-linking agents on the acoustic admittance; nonlinear response properties; and propellant burning rate. Concurrent theoretical studies have been directed toward predicting the effects of these reactions on the acoustic response function. These studies have included the study of the influence of pressure-dependent heat transfer from the gas phase combustion zone, the effects of various combustion parameters, and the investigation of sub-surface reaction contributions. This report presents the results which have been obtained during the second year of study.

2.0 TECHNICAL DISCUSSIONS

Recent studies on the structure of the combustion zone of composite solid propellants have presented indications that there are exothermic processes which occur on and within the solid phase.^{(1 through 6)*} The results of these studies indicate that the combustion process is controlled by two interdependent exothermic reaction zones near and on the surface of the propellant. One zone is in the gas phase at a finite distance from the solid propellant surface and is characterized by interdiffusion of gasified oxidizer and fuel species and combustion of particles of ejected matter from the surface. The second reaction zone occurs on and within the solid propellant surface. The primary heat release in this zone can occur as a result of exothermic decomposition processes and chemical reactions between the initial decomposition products of the solid oxidizer and the adjacent fuel surface. Transient and steady-state combustion studies indicate that much of the pressure-dependent combustion process can be associated with these interfacial reactions.

The exothermic surface reactions at and within the surface release sufficient heat to expel partially combusted products, pyrolysis products, and fuel and oxidizer fragments into the gas phase zone above the surface, where they intermix and burn completely. The maximum flame temperature is reached in the luminous zone, where the largest portion of the heat is released. However, because of the relatively large mass flow perpendicular to the surface, only a small amount of heat released in the luminous flame zone can normally reach the surface to supplement the heat generated by the interfacial reactions.

Incorporation of the exothermic chemical processes on and within the solid phase represents an important addition to the analysis of propellant combustion phenomena. Previous theoretical treatments of steady-state combustion^(7,8,9,10) as well as combustion instability^(11,12) have considered the exothermic combustion reactions to occur only in the gas phase. However, Friedly^(13,14,15) and Capener⁽¹⁶⁾ have shown theoretically that the principal time lags in the combustion zone are associated with energy transport within the solid phase for oscillations below 10,000 cps. By comparison, the time constants associated with the reaction and transport processes in the gas phase are small and these processes can be considered to be in equilibrium at any instant. Because the reactions on and below the surface are exponentially dependent on the solid phase temperature, the energy release by these reactions should be an important consideration in the analysis of transient combustion phenomena. Furthermore, the reported data indicate that these reactions on and within the solid phase are first order in local pressure.⁽⁴⁾ Thus, the acoustic pressure oscillations will produce oscillations in reaction rates through both the pressure and temperature sensitivities of the reaction rates which can have a significant effect on the combustion stability.

* Parenthetical superscript numbers denote references appearing on page 42.

2.1 EXPERIMENTAL STUDIES

The experimental studies conducted as part of the research program were directed toward investigating the effects of propellant combustion variables on the response of the combustion process to acoustic pressure oscillations. The principal propellant property derived from these studies was the real part of the acoustic response function, $\text{Re}(\mu/\epsilon)$, which relates the amplitude of the burning rate oscillations to the amplitude of the incident acoustic pressure oscillations by the relation

$$\text{Re} \left(\frac{\mu}{\epsilon} \right) = \frac{(\tilde{r}/\dot{r}_o)}{(\tilde{P}/P_o)} \quad (1)$$

2.1.1 Experimental Apparatus

Measurements of the acoustic response function were obtained in a T-burner apparatus. This type of equipment, which has become almost standard for acoustic measurements, consisted of a cylindrical combustion chamber with end-burning charges of propellant in either or both ends. The apparatus used in these studies was based on the design concepts of Horton⁽¹⁷⁾ and Stittmater⁽¹⁸⁾ and has an internal diameter of 1.5 in. over the entire length. Propellant samples are located in end caps which also contain provision for the igniter leads and pressure transducers. Electrically heated nichrome ignition wires are soldered to two electrodes which, in turn, are located in a ceramic tube inside the cap and pressure sealed with a connax fitting. The nichrome wire is passed through the propellant sample and is secured to the surface with small staples. Powdered propellant is then placed over the wires. Combustion products and pressurized gas are exhausted into two blowdown tanks through four orifices equally spaced around the circumference. Details of the apparatus, experimental procedure, and the electronic data acquisition system have been reported previously.⁽¹⁹⁾

The relationship between the observed acoustic pressure oscillations and the acoustic response function of the propellant has received considerable attention.^(17,18,20) Although several methods have been developed to derive the acoustic response function from acoustic pressure measurements, the only method used in this study was based on growth and decay constant determinations. Hence, the expression used to reduce the oscillating pressure measurement to the acoustic response function is

$$\text{Re} \left(\frac{\mu}{\epsilon} \right) = \frac{P_o}{4c \rho_s \dot{r}_o} \left[\frac{\alpha_g}{f_g} - \frac{\alpha_d}{f_d} \right] \quad (2)$$

During the experimental program, special care was required when tests were conducted at low frequencies. Under these conditions, the combustion chamber becomes long and the quantity of room temperature gas required to pressurize the chamber thereby becomes significant. After ignition, a significant period of time is required to achieve thermal equilibrium in

the combustor. However, the frequency of the pressure oscillations depends on the temperature through the sonic velocity, i.e., $c \sim \sqrt{T}$, and the expression

$$f_g = c/2L \quad (3)$$

One point worthy of note is that the sonic velocity which appears in equation 2 results from considerations at the combustion zone and therefore should be evaluated from the experimental flame temperature. The approach used in this study is based on the assumption that at high frequencies (short combustion chamber), the experimental flame temperature is established throughout the combustion chamber very rapidly. Thus, c was evaluated from equation 3 by extrapolating the parameter $2Lf_g$ to high frequencies

2.1.2 Propellant Formulations

There are several potential methods for controlling the contributions of surface reactions to the acoustical response. One method involves coating the oxidizer crystals with coating materials in an attempt to alter the reactivity of the crystal-binder interface. This approach, which was examined during the first year of effort, has been extended during the second year. The details of the coating and propellant preparation have been presented by Brown, et al.⁽¹⁹⁾

In addition to the effects of coatings, changes in the chemical structure of the binder and in the agents used to crosslink the binder were suspected of having a significant influence on the acoustic response function. Accordingly, propellants were prepared which permitted investigation of these variables.

The particular propellant formulations tested and the resultant burning rate data are shown in table I. Burning rate measurements were made in a standard strand burner at three pressure levels: 200, 500, and 1,000 psig. The data for each system were checked at the 200-psig level with the total burning time measurements in the T-burner, i.e., sample size with 1/4-in.-thick samples. The difference between the two values was less than 10% in all cases. Because of the experimental scatter in the burning rate measurements, these data are valid to within $\pm 10\%$ of the reported values. Also, the reported burning rate pressure exponents are abnormally high, especially considering the large oxidizer particle size which was used. However, the data at higher pressures show the exponents for many of these propellants are not constant over the entire range.

2.1.3 Experimental Results

During the second year of study, the acoustic response function of propellants 10 through 15 were determined as a function of frequency in the T-burner. These data are presented in figures 1 through 7 using the normalized frequency $8 \pi f_g / \bar{r}_0^2$ as the parameter. This form was used based on the theoretical studies of Hart⁽¹¹⁾ and Friedly⁽¹³⁻¹⁵⁾ and the theoretical studies to be discussed in the sections that follow. These

TABLE I
PROPELLANT FORMULATIONS USED TO TEST COATING EFFECT

Propellant No.	Formulation No.	Composition % Binder/ % Oxidizer	Oxidizer Particle Size	% Polymer	Oxidizer Coating % Additive	Propellant Additive	Rate at 200 psi in./sec	Rate at 200 psi	Binder/Curing time
1	UTX-8501-2	22/78	190	0	0	0	0.113	0.79	CTPB/MAFO
2	UTX-8502-1	22/78	190	1.5 Kel-F	0	0	0.116	0.75	CTPB/MAFO
3	UTX-8525-1	22/78	100	0	0	0	0.129	0.60	CTPB/MAFO
4	UTX-8526-1	22/78	190	1 Kel-F	1 Cab-O-Sil	0	0.170	0.64	CTPB/MAFO
5	UTX-8527-1	22/78	190	1 Kel-F	2 LfF	0	0.063	0.79	CTPB/MAFO
6	UTX-8528-1	22/78	190	1.5 Hypalon	0	0	0.128	0.87	CTPB/MAFO
7	UTX-8529-1	22/78	190	1.5 Ethyl Cellulose	0	0	0.137	0.69	CTPB/MAFO
8	UTX-8531-1	22/76.5	190	0	0	0.77% Kel-F 0.77% Cab-O-Sil	0.158	0.53	CTPB/MAFO
9	UTX-8532-1	22/76.8	190	0	0	1.2% Kel-F	0.110	0.75	CTPB/MAFO
10	UTX-9164-1	22/78	190	3.0 Kel-F	0	0	0.120	0.66	CTPB/MAFO
11	UTX-9165-1	22/78	190	1.5 Viton A	0	0	0.108	0.65	CTPB/MAFO
12	UTC-9167-1	22/78	190	0	0	0	0.145	0.66	PBAN/EPOXY
13	UTX-9168-1	22/78	190	0	0	0	0.127	0.50	PBAN/MAFO
14	UTX-9173	22/78	190	0	0	0	0.138	0.42	CTPB/EPOXY
15	UTX-9368	16/84	70 MS-4 30 Fines	0	0	0	0.126	0.30	UTREZ

theoretical studies suggest that the proper form for the dimensionless frequency should include the propellant thermal diffusivity. For the propellant listed, this propellant property should be relatively constant (approximately 3×10^{-4} in.²/sec) and therefore has been omitted. In addition, the definition of the acoustic response function is such that it should approach the normal burning rate pressure exponent as the frequency approaches zero; therefore, the data are reported showing the extrapolation at low frequencies to the burning rate pressure exponent obtained from the burning rate measurements.

For completeness, all the experimental data obtained for all the propellants shown in table I are presented in appendix A. The values of the growth frequency (f_g), growth rate (α_g), decay frequency (f_d), decay rate (α_d) and $\text{Re}(\mu/\epsilon)$ are reported with the graphs of the data showing the acoustic response as a function of the measured growth frequency.

It is important to note that the data are subject to significant uncertainty. The steady-state burning rates, as previously indicated, may have errors as high as $\pm 10\%$. These values enter into the calculation of the response functions, i.e., $\mu \propto 1/\dot{r}_0$, and the frequency functions, $8\pi f_g/\dot{r}_0^2$. In addition to these uncertainties, the measurements of the growth and decay rates are subject to an uncertainty of $\pm 10\%$; therefore, the absolute value of the response function μ/ϵ is valid to within $\pm 20\%$. The experimental results must be interpreted accordingly.

The data obtained using the propellants containing 3% Kel-F and 1.5% Viton A-coated AP are shown in figure 1, together with previously reported data on the 1.5% Kel-F-coated AP and the 1.2% Kel-F in the binder. The effect of these coatings on the maximum admittance is significant. Coating the oxidizer with Kel-F 800 reduced the maximum admittance by 50% compared to the uncoated oxidizer. Increasing the level of coating further reduced the response function, although the reduction does not increase linearly with coating level. The effect of the Kel-F coating on the magnitude of μ/ϵ is consistent with the concept of interfacial reactions because Kel-F is more resistant to oxidation than the CTPB binder. However, the data reported previously⁽¹⁹⁾ on the effects of other coatings (Hypalon 30 and ethylcellulose) showed no effect of the coating on the maximum acoustic response function. Apparently, only the Kel-F and Viton reduced the reactivity of the exothermic reactions in the solid phase sufficiently to have a significant effect on the response properties.

Because both these materials contain halogen, one is tempted to conclude that the presence of halogen is responsible for the changed behavior. However, the data indicate that incorporating the Kel-F into the binder appears to have had very little effect on the response function. The observed effect is approximately a 10% increase, but this effect is less than the experimental error. Hence, the location of the additive is also important and it is postulated that the contribution of interfacial reactions to the overall combustion process is in part reduced by the coating, which in turn reduces the admittance.

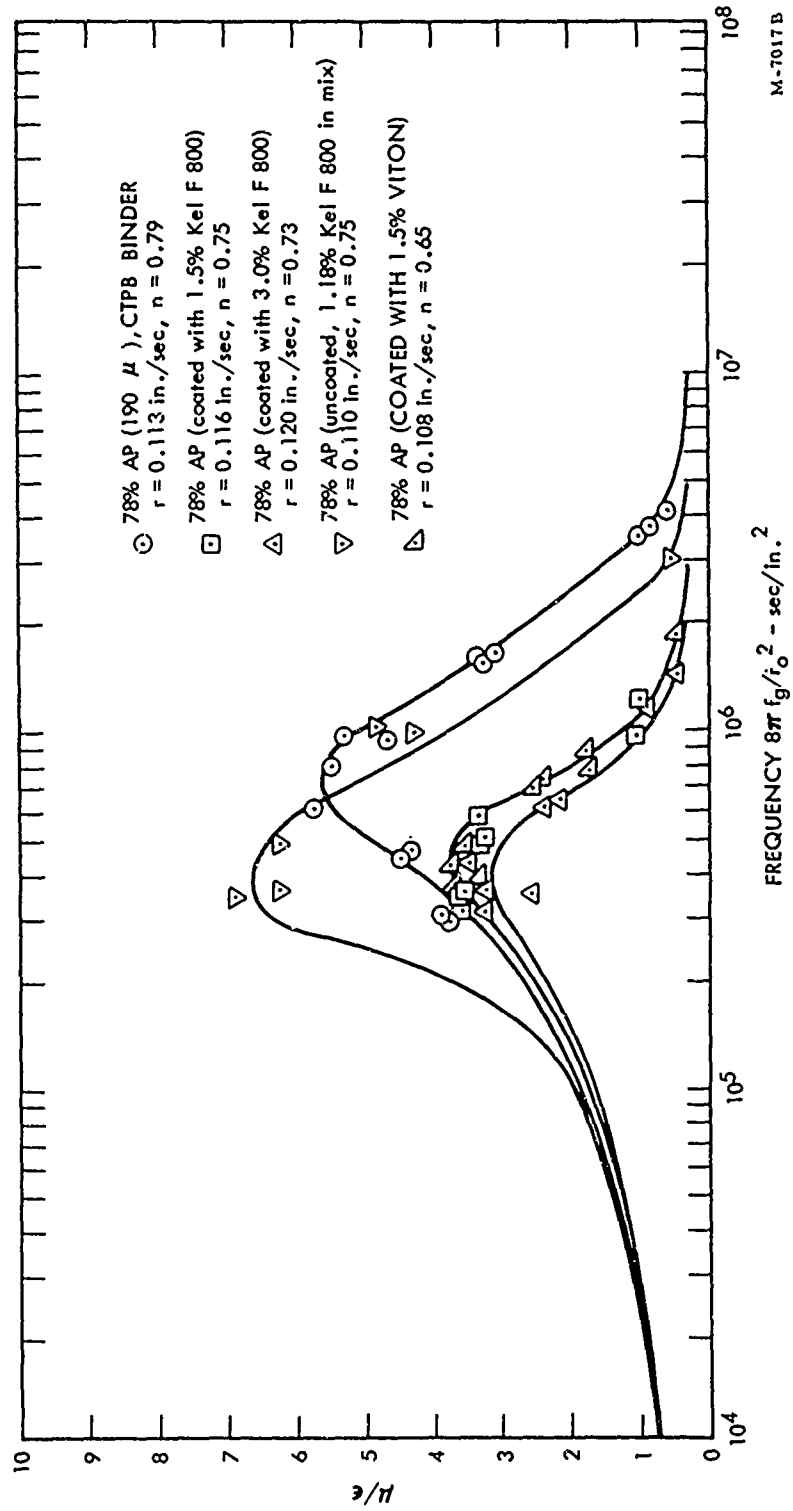


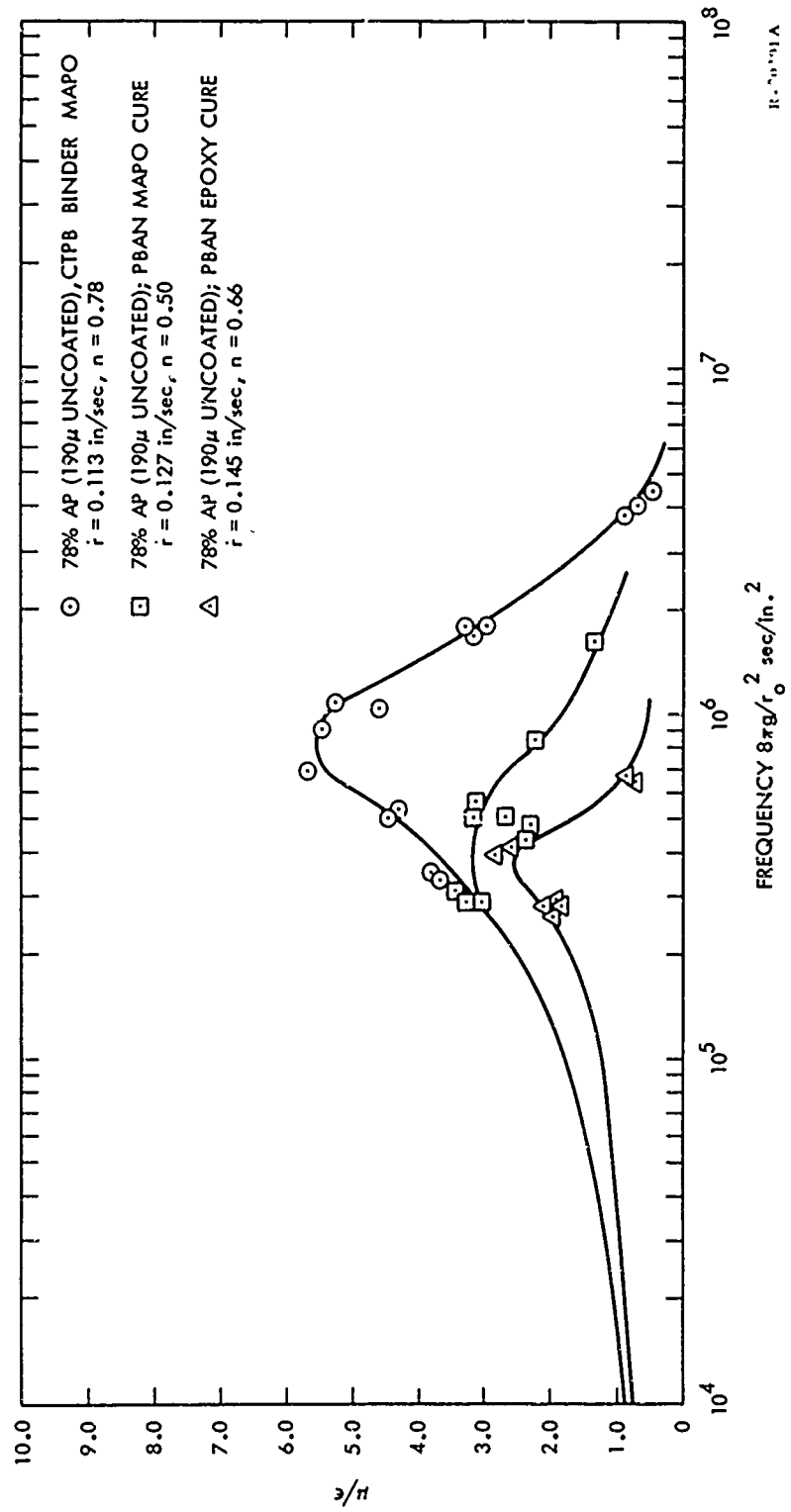
Figure 1. Effect of Kel-F and Viton Coatings on Acoustical Response

Also, it is interesting to note that the burning rate and the burning rate pressure exponent for the standard propellant, as well as the Kel-F-modified and Kel-F-coated AP essentially are identical. When compared with the acoustic response data, these results would suggest that the postulated effect of interfacial reactions is more significant under transient combustion conditions than under steady-state conditions.

Another aspect of the experimental studies was concerned with the large difference between the results obtained by Horton⁽²¹⁾ and the propellants tested in this study. The maximum acoustic response of about 6 was found for the CTPB propellants, where Horton observed the maximum of about 3 for the PBAA propellant. It appears that the binder has a significant effect on the acoustic response function. To study this effect in greater detail, propellants were prepared in which the CTPB binder was replaced by PBAN cured with MAPO in one case and with epoxides in another. The results are shown in figure 2 for both the MAPO cross-linked binder (UTX-9162) and the epoxy cross-linked propellant (UTX-9168). The epoxy-cured propellant had a burning rate at 200 psig of $\dot{r} = 0.145$ in./sec and the MAPO-cured propellant of $\dot{r} = 0.127$ in./sec. For comparison, the data for the MAPO-cured CTPB propellant are also shown in figure 2 and indicate that a change of binder reduced the acoustic response significantly. Because the magnitude of the response function measured by Horton on PBAA propellants and these data are nearly equal, these results suggest that the data appear to be consistent between the two T-burners. It would appear that the choice of the CTPB binder was particularly fortunate for studying the additive effects. It also appears that CTPB propellants have somewhat higher acoustic response functions, at least for nonaluminized AP formulations loaded to 75% to 78%.

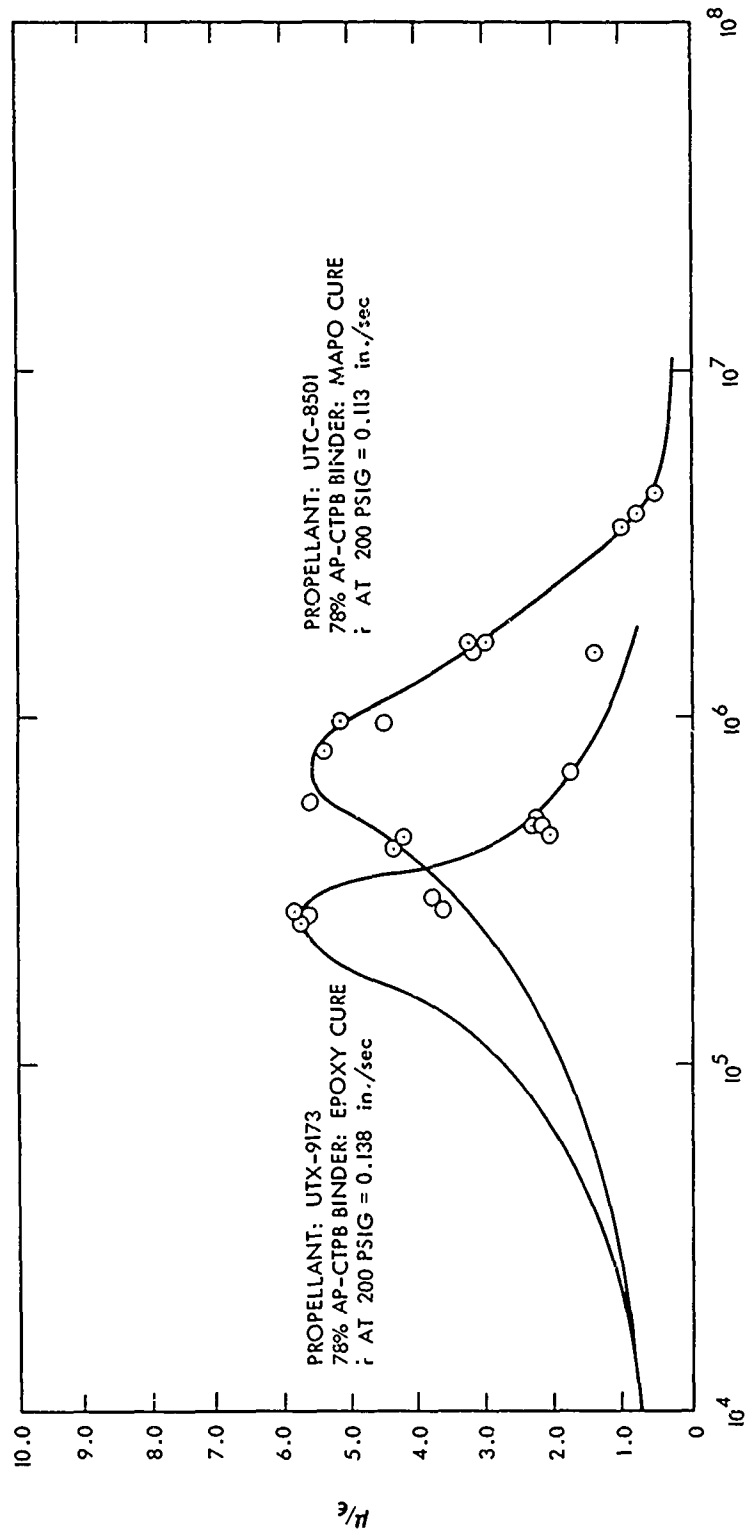
The effect of changing the MAPO curing agent used in the previous studies⁽¹⁹⁾ to an epoxy system has been also studied using the standard CTPB propellant formulation with noncoated oxidizer. The response functions for UTX-9173 are shown in figure 3, which was an epoxy-cured CTPB propellant (78% AP), along with the basic formulation UTX-8501 (78% AP in CTPB binder-MAPO cure). The epoxy-cured propellant had a burning rate at 200 psig of $\dot{r} = 0.138$ in./sec and the MAPO-cured propellant was $\dot{r} = 0.113$ in./sec. The results indicate that the position of maximum acoustic response occurs at a lower frequency for the epoxy-cured propellants. However, the maximum value of the acoustic response function is not significantly altered by the change in the cure system.

Two observations can be made from these results. First, the acoustic admittance for the PBAN propellants are significantly less than those of the equivalent CTPB propellant. Secondly, the admittance of the epoxy-cured propellant is less than the admittance for the MAPO-cured PBAN propellant. This latter effect was not observed with the CTPB propellant. Thus, there appears to be an interaction between the cure agent and the binder such that cure agent effects depend on the binder. The mechanisms responsible for this interaction are not immediately apparent and further study is required to explain these observations.



R-20001A

Figure 2. Effect of PBAN Binders



7077A

Figure 3. Response Functions for UTX-9173

The effect of ambient pressure on the acoustic admittance function was also studied using the basic 78% AP-CTPB binder propellant. Pressures of 100, 200, and 500 psig were investigated and the results are shown in figure 4. The dimensional frequency $8 \pi f_g / \dot{r}^2$ is based on the burning rate of the propellant at the specified pressure. The data indicate that, over the range of pressures studied, the maximum value of $\text{Re}(\mu/\epsilon)$ increased as the pressure increased (i.e., compare 200 and 500 psig). This latter effect is caused by \dot{r}^2 factor in the dimensionless frequency ($8 \pi f_g / \dot{r}^2$).

To compare these results with pressure data obtained on a 76% AP (80 μ): 24% PBAA propellant by NOTS, (22) the response function at the various pressure levels is shown as a function of the measured growth frequency in figure 5. The results are consistent with the observations by NOTS in that the greatest shift in the frequency at which the maximum appears in the response function occurs between 100 and 200 psig and only a small change occurs between 200 and 500 psig

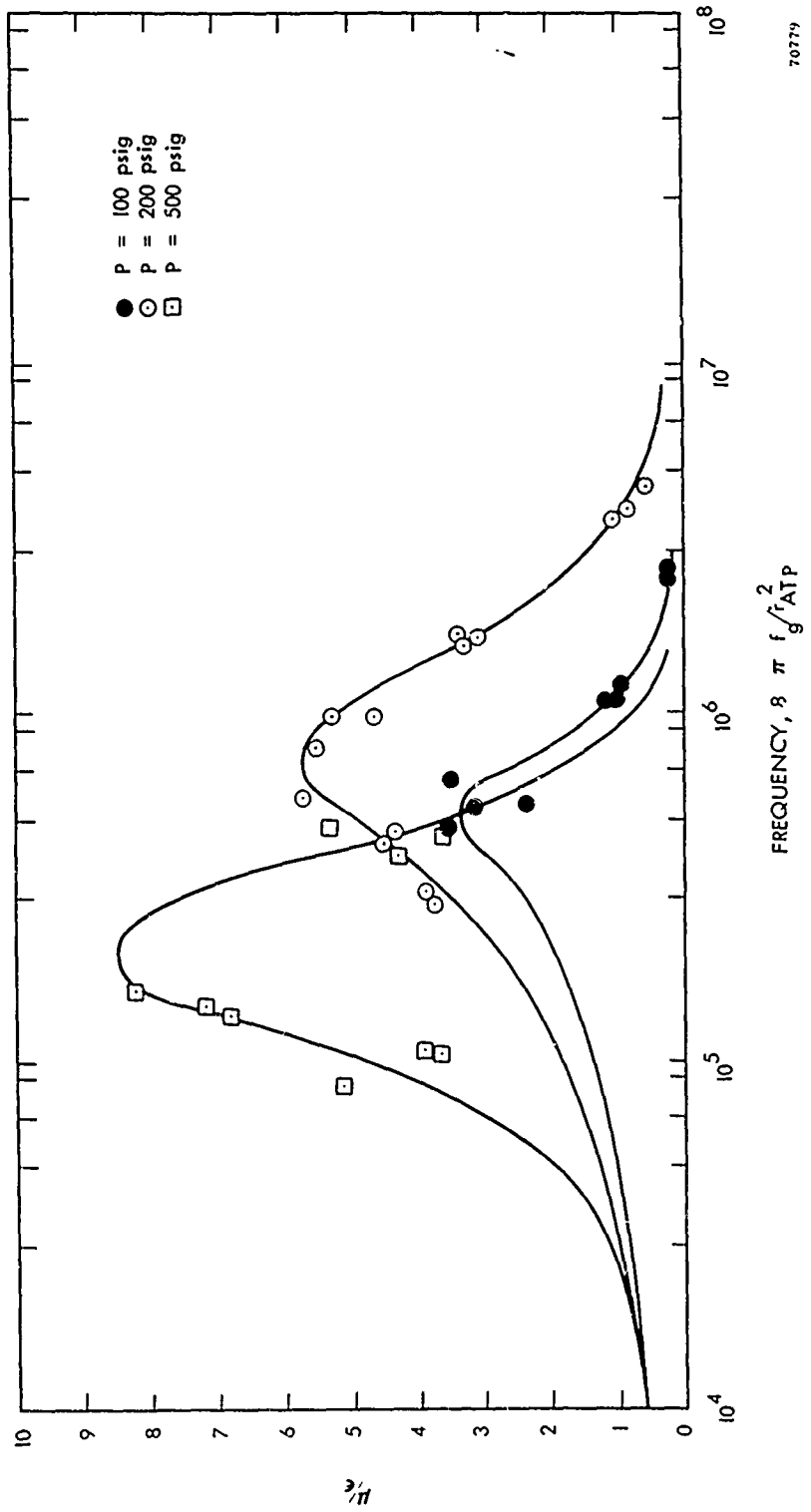
Data were obtained on NOTS propellant A-13 in connection with the round robin for the Standardization Committee on Combustion Instability Measurements and was presented at the committee meeting on 6 June 1967 at Anaheim, California. The data were obtained over a frequency range from 250 to 4,000 cps at a chamber pressure of 200 psig and are tabulated in appendix A. A comparison of these results with the earlier work of Horton (21) is shown in figure 6. The results agree favorably over this frequency range. In the frequency range from 1,000 to 4,000 cps, the present results were also consistent with the majority of investigators on the committee.

Further experiments were conducted with a 84% AP-UTREZ (polyisobutylene) binder. (This propellant was prepared for the photographic studies discussed in section 2.1.4.) The acoustic response data for the UTREZ propellant are shown in figure 7 with the data from the standard 84% AP-CTPB binder; both propellants were cured with the same curing agent. The burning rate of the UTREZ propellant was 0.125 in./sec, and the CTPB propellant had a value of 0.113 in./sec at 200 psia. However, both the oxidizer loading as well as the binder type were varied. Current studies include measurement on a 84% AP-loaded UTREZ propellant and the significance of the available data cannot be determined until further data can be obtained.

2.1.4 Photographic Studies

The theoretical model for the combustion process depends on a knowledge of the chemical and fluid mechanical processes which influence the acoustic admittance. The previously discussed T-burner experiments have been useful in determining the effects of propellant changes on the measured pressure-time variations (i.e., acoustic admittance), but it is difficult to resolve the details of the combustion behavior from these types of indirect observations. Therefore, it is desirable to examine the propellant when it is burning under oscillatory conditions in the T-burner.

A sample holder was constructed with viewing windows as shown



70779

Figure 4. Effect of Pressure on Acoustic Response

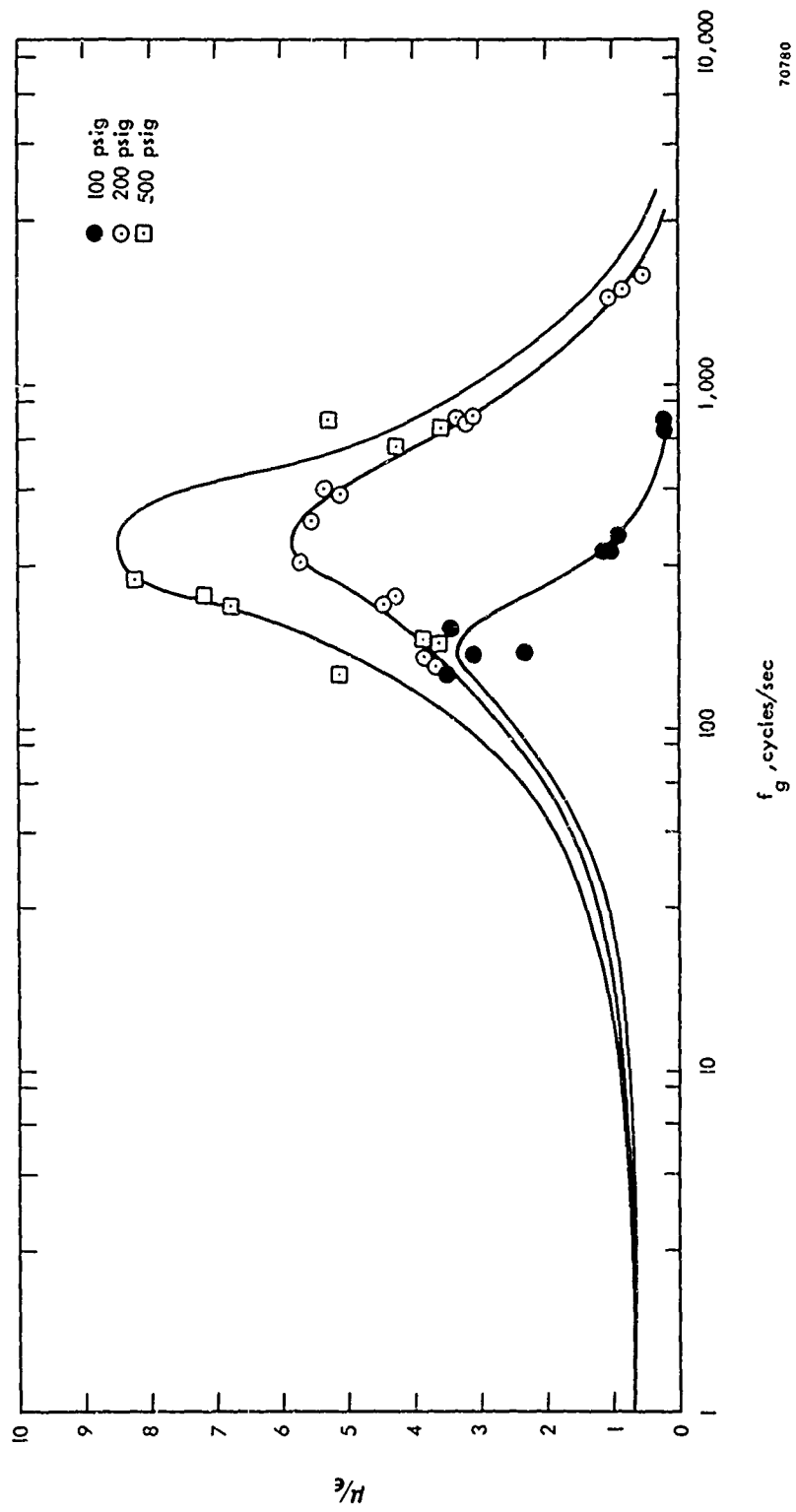
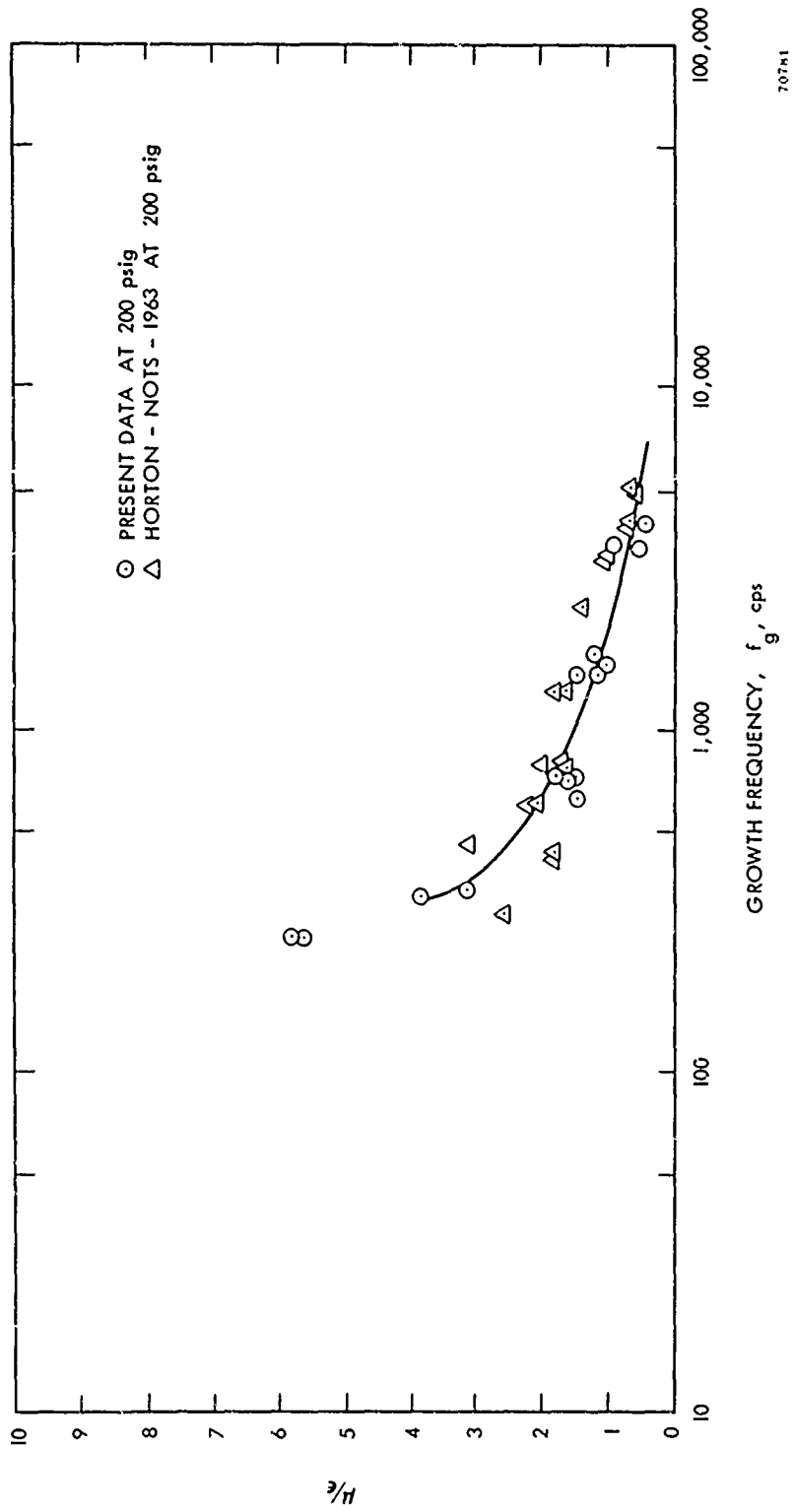
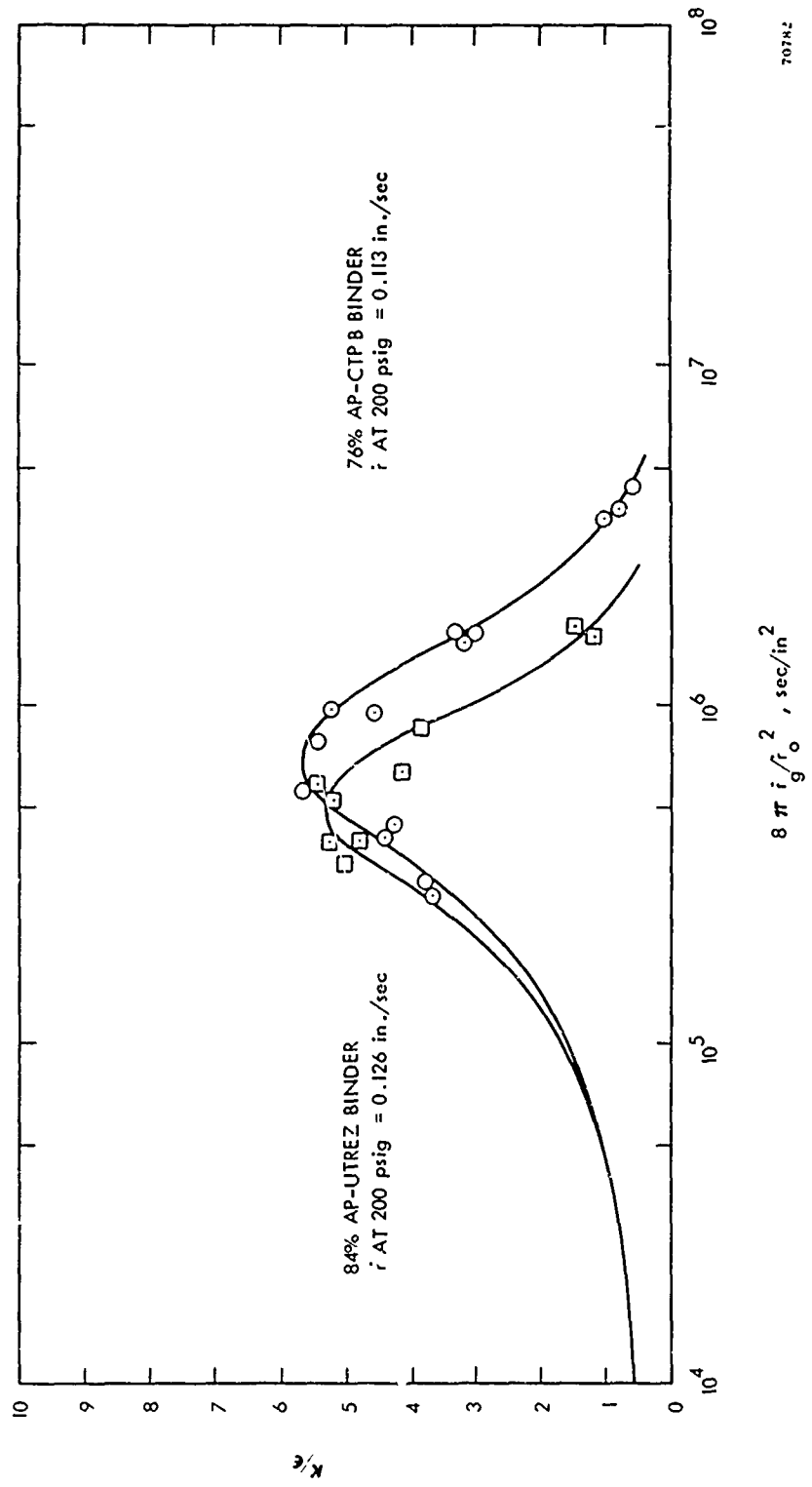


Figure 5. Effect of Pressure on Acoustic Response



707M1

Figure 6. NOTS A-13 Propellant Data



70782

Figure 7. Acoustic Response of CTPB and UTREZ Binders

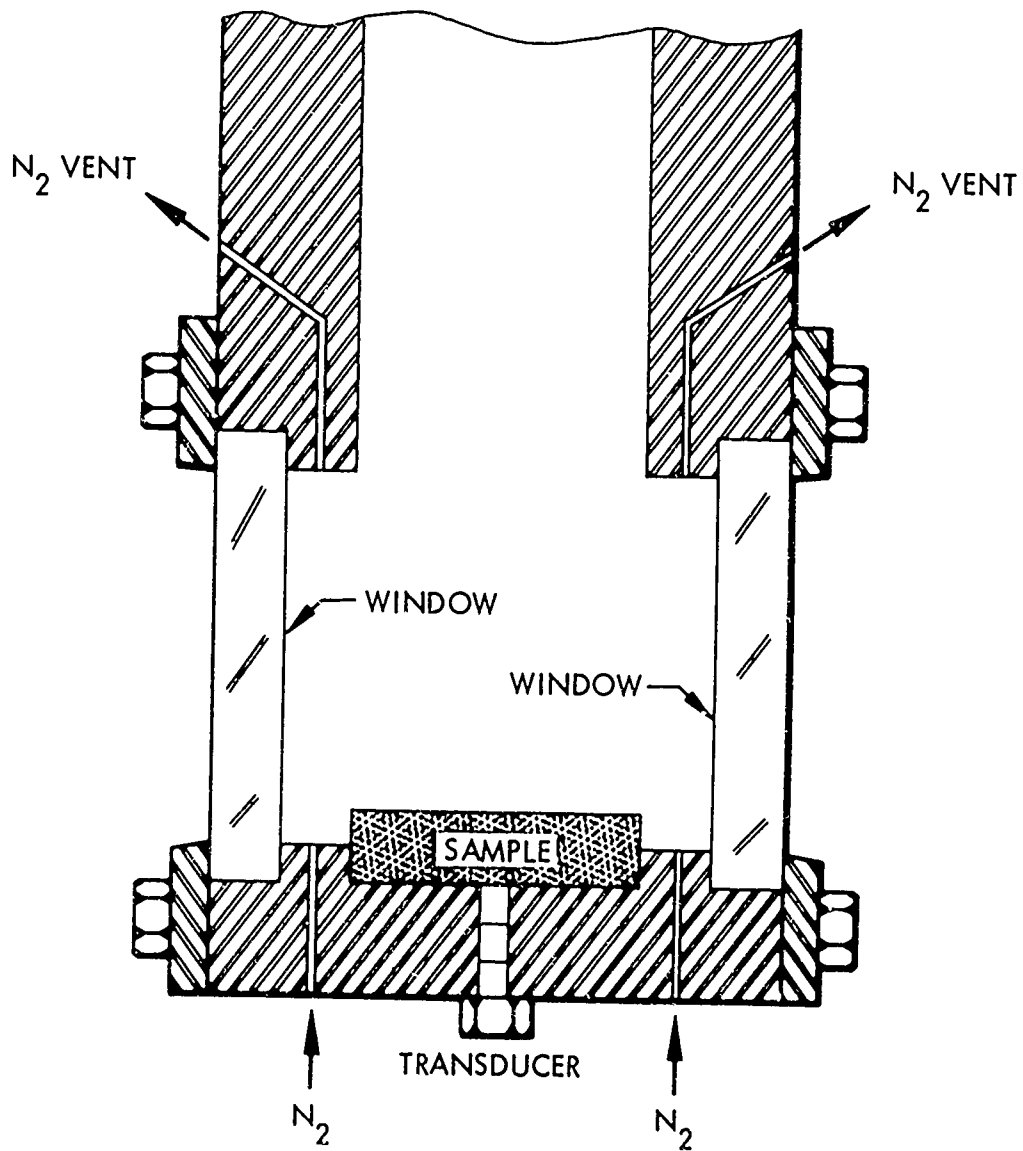
schematically in figure 8. The 1-1/2-in.-diameter propellant disk is located in the center and a purge system is placed between the sample and the windows. Tests were conducted using both Vycor and Plexiglas windows with and without the purge system. The windows were sealed to their mounting with gaskets. A photograph of the final assembly is shown in figure 9.

The camera used in these studies is a Hycan 16-mm rotary prism camera with a framing rate capacity to 4,000 frames/sec, which will provide several frames during a complete cycle at the lower frequencies. The initial photographs were taken at a framing rate of 500 frames/sec. A quartz-iodine lamp was used for backlighting the viewing section. The complete camera arrangement is shown in figure 10.

The greatest problem encountered in the photographic studies is the rapid buildup of carbonaceous material on the windows. To eliminate this problem, several changes were made in the experiments. A "clean burning" propellant consisting of 84% AP was selected. The burning rate at 200 psig is 0.130 in./sec. The windows were also recessed from the tube walls to allow the nitrogen window purge to operate efficiently. The amount of ground propellant placed over the ignition wires was reduced to minimize the effects of the additional mass ejected during the ignition phase and subsequent clouding of the windows.

These changes significantly improved the initial photographic results and made it possible to observe the propellant surface during a large portion of the run. During the early stages, a film of opaque material is temporarily deposited on the windows, thereby preventing observation of the initial stages of the instability process. Methods of solving this problem are currently being considered.

A typical film sequence is shown in figure 11 for the 84% AP propellant. The sides of the test sample were inhibited before firing and a nitrogen purge was used in this test. The photographs were taken from the 16mm color film, and the original film displays greater detail than appears in figure 11. Random frames were selected to display various features of the combustion process. The first frame shows the test section before firing and the next frame displays the ignition process. Ignition is obtained by electrically heating the nichrome wire secured to the propellant surface and this appears as a blue flash (i.e., bright flash near surface in frame 2) when the electrical contact is broken. Once ignition has occurred, mass is evolved from the surface as displayed by the luminous streaks near the surface in frame 3. At a later time, the propellant started to burn around the inhibitor, as shown in frames 4 and 5; this particular problem is presently under investigation.



70783

Figure 8. Schematic of Viewing Section



Figure 9. Photograph of Viewing Section

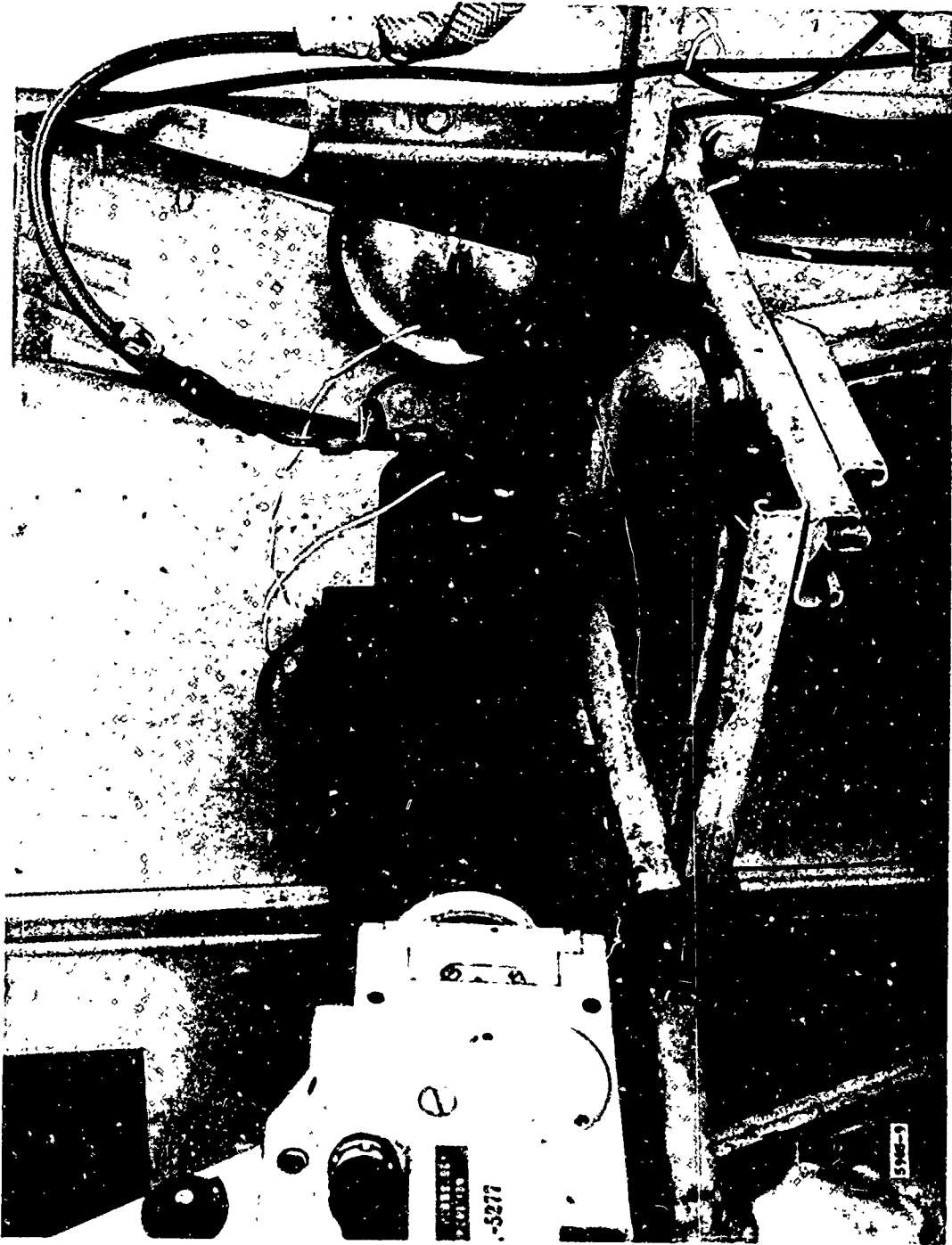
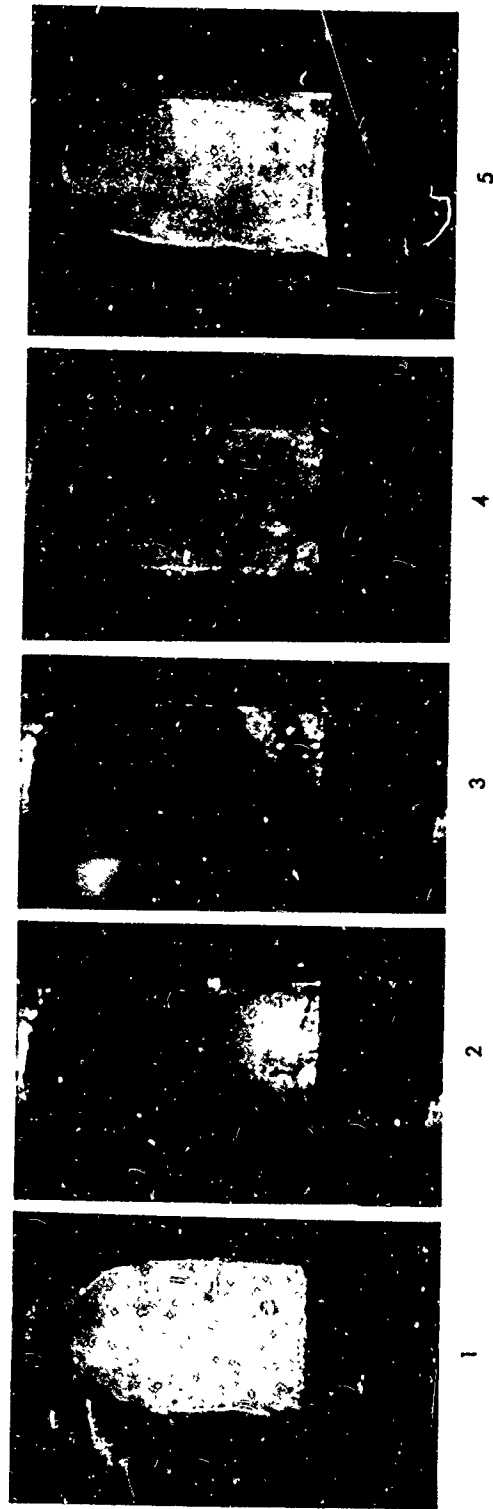


Figure 10. Camera Arrangement for Viewing Section



26786

Figure 11. Photograph of Combustion Process in T-Burner Viewing Section

2.2 THEORETICAL STUDIES

The theoretical study of the approximate combustion model reported in the first technical summary report (UTC 2136-TSR1) has been continued in order to improve the basis for interpretation and correlation of the experimental data. These studies were motivated by two considerations. First, previously reported theories have not accounted for the magnitude of the response functions found experimentally in this program and those reported by Horton.⁽²¹⁾ Second, earlier studies have not considered the effects of exothermic surface reactions of the type discussed in preceding paragraphs. Without a suitable theoretical framework, it has not been possible to determine any contribution of exothermic surface reactions on the acoustic response function. Therefore, development of a model which included surface reaction effects was initiated.

The approach taken in these studies has been to formulate a simplified analysis to facilitate the study of the overall linear behavior of the model. In addition, these studies will permit estimation of the important nonlinearities, i.e., burning rate changes, sinusoidal wave forms, and variation of admittance with pressure amplitude. The analysis is intended to be expanded at a later date, as dictated by the experimental data and the results of the preliminary theoretical analysis, to study the more important processes in detail.

During this past year of study, the basis for the model has been refined, the linear solutions have been studied in greater detail, and the nonlinear behavior has been studied further. The following paragraphs present new developments in these areas.

2.2.1 Analytical Combustion Model

From the description of the combustion zone, the transient behavior of the solid phase can be modeled, at least to a first approximation, by the one-dimensional form of the transient heat conduction equation expanded to include the effects of exothermic reactions. This equation is

$$\frac{\partial T}{\partial t} = \alpha \frac{\partial^2 T}{\partial x^2} + \dot{r} \frac{\partial T}{\partial x} + Z_3 \exp(-E_3/RT) \quad (4)$$

At the surface of the propellant, a heat balance, as suggested by the qualitative description of the combustion zone discussed earlier, indicates that the total heat received by the surface is given by

$$-k \left(\frac{\partial T}{\partial x} \right)_{x=0} = F + Z_1 P \exp(+E_1/RT) - \Delta H_v \rho \dot{r} \quad (5)$$

(1) (2) (3)

The terms on the right-hand side of equation 5 represent:

- (1) = heat supplied from the flame zone (gas-phase reaction zone a finite distance away from the surface)
- (2) = heat generated at the surface by heterogeneous reactions between the solid oxidizer decomposition gases and the exposed fuel matrix
- (3) = heat released because of gasification of propellant at the surface

Before the oscillatory response to induced oscillations can be studied with the preceding equations, the effect of pressure on the gas-phase heat transfer must be considered. This effect, which has received attention in several studies, (7,8,23,24,25) is the result of a complex interaction between diffusional processes, which are independent of pressure, and chemical reaction processes, which are highly pressure dependent.

In recent studies, Denison and Baum, (25) Marxman, (24) and Friedly (13) have used approximate solutions of the laminar premixed flame equations to characterize the gas phase contributions. These equations generally have the form

$$\dot{q} \sim P^{\frac{m-1}{2}} T_f^{\frac{m+2}{2}} \exp(-E_f/RT_f) \quad (6)$$

Unfortunately the use of equation 6 results in two fundamental limitations. First, the transient analysis based on this equation predicts oscillations in the flame temperature. However, thermodynamic calculations show the flame temperature to be nearly independent of the pressure. Under the assumption of pseudoequilibrium in the gas phase, the flame temperature should also remain constant under oscillatory conditions as well. The only reasonable mechanism for a shifting flame temperature is a shifting oxidizer-to-fuel ratio, but such provision is not included in these analyses.

The second limitation concerns the applicability of the results to the experimental data obtained in the present studies. Equation 6 does not consider the heterogeneous nature or "unmixedness" of the composite propellant combustion zone. Though the combustion zone of double-base propellants is perhaps one dimensional, this certainly is not the case for composite propellants. To account for these effects, Summerfield (7) has suggested that the characterizing expression should be

$$F^{-1} = aP^{-1} + bP^{-1/3} \quad (7)$$

while Penner (23) has developed a more complex expression based on a slightly different approach but which yields the same approximate result as equation 7. It can be shown that equation 7 can be approximated over reasonable pressure ranges by

$$F = F_0 (P/P_0)^n \quad (8)$$

In view of the obvious simplicity of equation 8 over equation 7 and the approximate nature of equation 7, equation 8 was used to characterize the gas phase effects in the analytical development.

The heat generated by surface reactions has been incorporated into the surface energy balance, equation 5, by assuming the overall reaction is first order in pressure. This assumption is based on the observations of Anderson, et al, ⁽⁴⁾ which showed these reactions to be initially controlled by the rate of absorption of reaction species. More recently, Hermance ^(26,27) has shown theoretically that pressure-dependent surface reactions can contribute significantly to the overall combustion process in the intermediate pressure region between 100 and 1,500 psi. In view of these observations, it is reasonable to assume that the effects of these reactions can be incorporated as shown in equation 5.

The analysis also requires an expression relating the regression rate to the surface temperature. In these studies, it has been assumed that the linear burning rate is determined by some overall pyrolysis rate of the solid phase. Mathematically, this can be expressed

$$\dot{r} = Z_2 \exp(-E_2/RT_s) \quad (9)$$

In reality, equation 9 represents an approximation of the physically real situation in which several reactions are occurring simultaneously. Certainly, a more elaborate expression could be used where the burning rate is related to the weighted sum of a series of Arrhenius expressions. However, the hypergolic ignition studies of Anderson ⁽⁴⁾ have shown that significant energy release can result from interfacial reactions without substantial gasification of reaction products. Thus, to a first approximation, one would expect the principal effect of these reactions to affect the thermal balance at the surface and not the material balance. Mathematically therefore, the effects of these reactions have been included in equation 5 but are not explicitly shown in equation 9.

To complete this analysis, the temperature deep within the propellant remains constant at the initial propellant temperature. Mathematically, this can be expressed as

$$T = T_\infty \quad \text{at } x = \infty \quad (10)$$

Equations 4, 5, 8, and 10 represent an approximate one-dimensional model of the combustion zone. The equations are highly nonlinear, and solutions require finite difference methods and an electronic computer. By making certain approximations in these equations, an approximate solution for the linear response characteristics, i e., the acoustic admittance, can be developed to guide the interpretation of experimental data.

Baer, (28) in his analytical studies on ignition of solid propellants, has shown that it makes little difference whether the energy source term is in the boundary condition or in the basic differential equations. Physically, this approximation assumes that the solid phase reaction zone is concentrated near the propellant surface as a result of the high temperature gradient in the solid phase. Because the temperature gradient is high, this observation also should apply to analysis of combustion instability. Thus, as a further approximation, the energy source term in equation 4 can be eliminated, which yields

$$\frac{\partial T}{\partial t} = \frac{\partial^2 T}{\partial x^2} + \dot{r} \frac{\partial T}{\partial x} \quad (11)$$

2.2.2 Linear Response Studies

By letting

$$T(x,t) = T^0(x) + \theta_1(x,t) \quad (12)$$

where $\theta(x,t)$ is small compared to $T^0(x)$, equations 5, 8, 9, and 11 become

$$\frac{1}{4} \frac{\partial \theta_1}{\partial \tau} = \frac{\partial^2 \theta_1}{\partial \zeta^2} + \frac{\partial \theta_1}{\partial \zeta} - T^0 \theta_1(0) (1-\phi)\mu \exp(-\zeta) \quad (13)$$

$$\frac{\partial \theta_1(0,t)}{\partial \zeta} = T^0(0) \cdot (\eta n' + \Gamma) P/P_0 + T^0(0) \cdot (\Gamma \Lambda - \beta)\mu \quad (14)$$

$$\dot{r} = \dot{r}_0 (1 + \mu) \quad (15)$$

$$F = F_0 (1 + n' P/P_0) \quad (16)$$

Equation 13 can then be solved using Laplace transforms as suggested by Denison and Baum. (22) When the boundary conditions given by equation 13 are applied, the result becomes

$$\mathcal{L}(\tilde{\mu}) = \frac{-(\eta n' + \Gamma) \mathcal{L}(\tilde{P})}{M_1 (\psi + 4(1-\phi)/s) + \Gamma \Lambda \beta + 4(1-\phi)/s} \quad (17)$$

The acoustic response function for this simplified model of the combustion zone can be determined by investigating the oscillations in the burning rate produced by sinusoidal pressure oscillations of small amplitude, that is to pressures having the mathematical form

$$\tilde{P} = p_0 (1 + \epsilon_1 e^{i\omega t}) \quad (18)$$

Hence

$$\mathcal{L}(\tilde{P}) = \epsilon_1 / (s - a') \quad (19)$$

Substituting equation 19 and 17 yields

$$\begin{aligned} \epsilon_1 \left(\frac{\psi}{\Gamma + \eta n'} \right) = & \left[\frac{(1 + \sqrt{a_1}) \operatorname{erfc}(-\tau \sqrt{a_1})}{(\gamma_1 - a_1)(\gamma_2 - a_1)} + \frac{(1 - \sqrt{a_1}) \operatorname{erfc}(\tau \sqrt{a_1})}{(\gamma_1 + a_1)(\gamma_2 + a_1)} \right] e^{a\tau} \\ & + \frac{2\gamma_1(\gamma_1 + 1) \operatorname{erfc}(-\gamma_1 \sqrt{\tau}) e^{(\gamma_1^2 - 1)\tau}}{(\gamma_1 - a_1)(\gamma_1 + a_1)(\gamma_1 - \gamma_2)} \\ & + \frac{2\gamma_2(\gamma_2 + 1) \operatorname{erfc}(-\gamma_2 \sqrt{\tau}) e^{(\gamma_2^2 - 1)\tau}}{(\gamma_2 - a_1)(\gamma_2 + a_1)(\gamma_1 - \gamma_2)} \quad (20) \end{aligned}$$

where

$$\begin{aligned} \gamma_1 + \gamma_2 &= -2(1+R) ; R \equiv \frac{\beta - \Gamma \Lambda}{\psi} \\ \gamma_1 \gamma_2 &= (1 - 2R + 4S) ; S \equiv \frac{1 - \phi}{\psi} \quad (21) \end{aligned}$$

The steady oscillatory behavior, provided such a condition exists at all, can be obtained by an examination of equation 20 for large times.

2.2.2.1 Stability in Self-Excited Modes

To determine if steady oscillatory behavior does exist for a particular set of combustion parameters (i.e., $(\beta - \Gamma \Lambda) / \psi$ and $(1 - \phi) / \psi$), the behavior of the third and fourth terms in equation 20 must be examined. From these

two terms, it is apparent that these terms will disappear with time to produce a steady oscillatory response if either

$$\operatorname{Re} (\gamma_i^2 - 1) < 0 \quad (22)$$

or

$$\operatorname{Re} (\gamma_i^2 - 1) > 0 \text{ but } \operatorname{erfc} (-\gamma_i \sqrt{\tau}) \rightarrow 0 \text{ as } \tau \rightarrow \infty \quad (23)$$

From the properties of the complimentary error function having complex arguments and equations 21, 22, and 23, the regions of stable oscillatory behavior can be determined as a function of the parameters $(\beta - \Gamma\Lambda)/\psi$ and $(1-\phi)/\psi$. The resulting stability map is shown in figure 12 together with the relations between $(\beta - \Gamma\Lambda)/\psi$ and $(1-\phi)/\psi$ separating the two regions. Also shown are the regions in which the burning rate oscillations increase without limit, either in an oscillatory manner with exponentially increasing amplitude or exponentially without oscillation.

This figure shows that stable oscillatory behavior always occurs when $\beta > \Gamma\Lambda$, regardless of the temperature parameter $(1-\phi)/\psi$. Hence, if the net heat of pyrolysis of the propellant surface (a weighted average for typical binders and ammonium perchlorate for composite propellants) is sufficiently endothermic to counter the effects of exothermic pressure-dependent reactions, stable oscillatory behavior will occur. If not, then instability in the self-excited modes can occur (depending on $(1-\phi)/\psi$) in any combustor. All that is required is some pressure distribution to initiate the transient process.

It is interesting to speculate whether in fact any solid propellants have been prepared which are unstable in the self-excited mode. It seems reasonable to assume that minor pressure disturbances occur in any combustor, including the normal burning rate strand bomb. If the propellant is unstable to self-excited modes, these disturbances would then induce burning rate oscillations of increasing amplitude or an exponential increase in burning rate with time. These burning rate disturbances will continue until second order effects somehow limit the disturbances or until the propellant is consumed. In either case, it seems reasonable to expect erratic burning rate data at the very best. Thus, the principal value in studying self-excited instability is that it provides a bound on the combustion parameter $(1-\phi)/\psi$ and $(\beta - \Gamma\Lambda)/\psi$ which cannot be violated when analyzing experimental acoustic response function data.

2.2.2.2 Acoustic Response Function

Having now determined the regions of steady oscillatory behavior, equation 18 can then be reduced to permit prediction of the acoustic response function. To perform this calculation, equation 2 suggests that one should use a complex frequency (i.e., $\alpha_g + i 2 \pi f_g$) in equation 20 to obtain

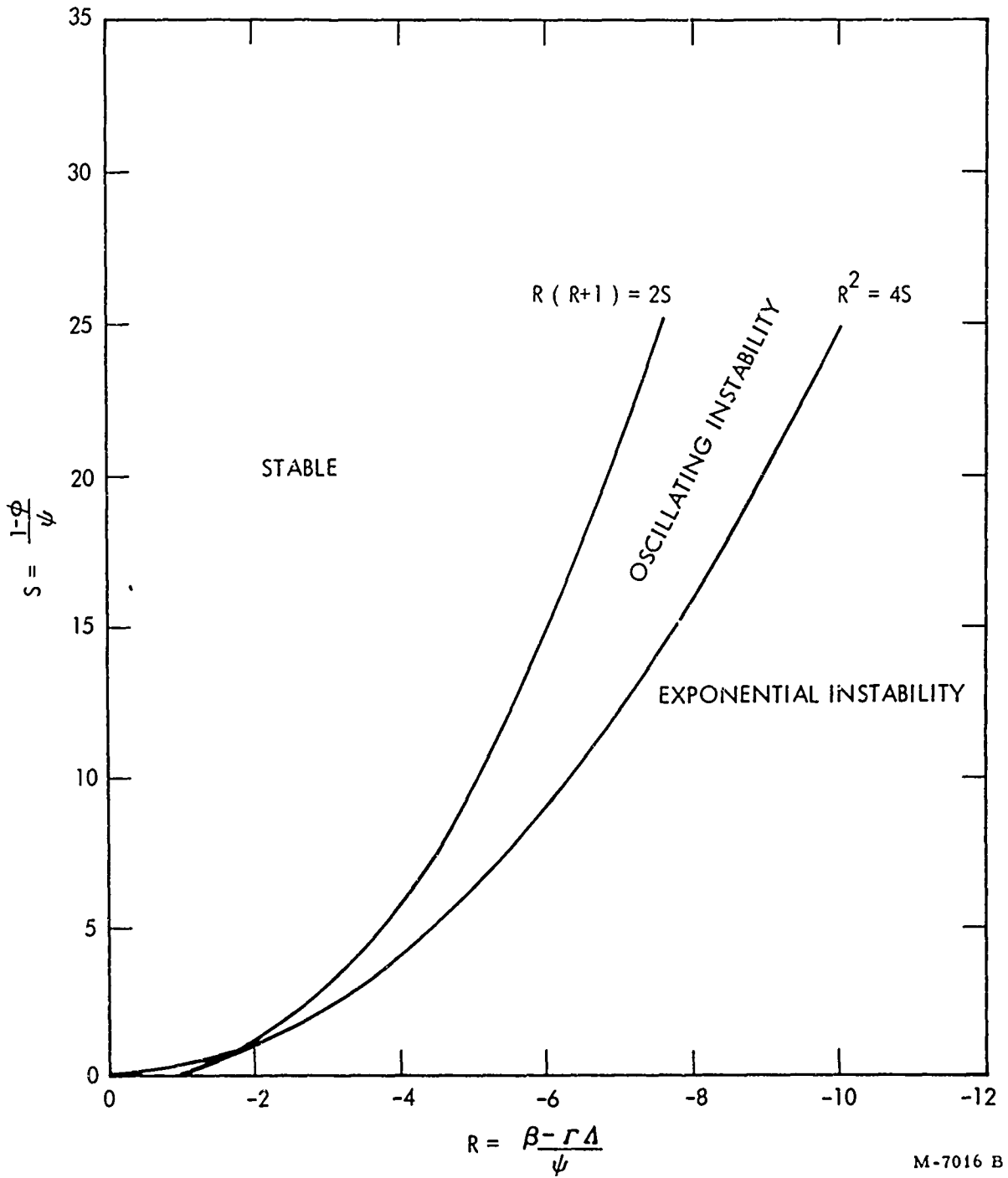


Figure 12. Stability Map for Self-Excited Modes

meaningful comparison between theory and experiment. This would account theoretically for the effects of the conditions of constantly increasing amplitude of the pressure disturbance which are used experimentally to evaluate acoustic response functions. However, assuming $P = 200$ psi, $c = 3,000$ ft/sec, $\rho = 0.06$ lb/in.³, $f_0 = 0.15$ in./sec, and $Re(\mu/\epsilon) = 6$, equation 2 indicates

$$\alpha_g / f_g = 0.1$$

Therefore, one can theoretically study the response to fixed-amplitude pressure oscillations and compare the results to experimental data obtained under conditions of constantly increasing amplitude, at least for the test conditions and propellants studied in this program. Hence $\omega = i 2\pi f_g$ can be substituted into equation 20 to yield

$$\frac{\mu}{\epsilon} \left(\frac{\psi}{\Gamma + \eta n'} \right) = \left\{ \left[1 + \frac{4(1-\phi)}{i \lambda \psi} \right] \left[\frac{1+(1+i\lambda)^{1/2}}{2} \right] + \left(\frac{\beta - \Gamma \Lambda}{\psi} \right) - \frac{4(1-\phi)}{i \lambda \psi} \right\}^{-1} \quad (24)$$

In addition to predicting the steady oscillatory response properties of the combustion model, equation 24 may be used to predict the theoretical pressure exponent of the steady-state burning rate, i.e., n in the equation

$$\dot{r}_0 = a P_0^n \quad (25)$$

From equations 1 and 24

$$n = \text{Lim Re}(\mu/\epsilon) = \frac{(\Gamma + \eta n')/\psi}{1 + \frac{\beta - \Gamma \Lambda}{\psi} + \frac{1-\phi}{\psi}} \quad (26)$$

These results indicate the acoustic response (μ/ϵ) - frequency (λ) relationship is a function of three parameters $\left(\frac{\psi}{\Gamma + \eta n'} \right)$, $\frac{4(1-\phi)}{\psi}$, and $\frac{\beta - \Gamma \Lambda}{\psi}$ or

n , $\frac{4(1-\phi)}{\psi}$, and $\left(\frac{\beta - \Gamma \Lambda}{\psi} \right)$. A parametric investigation of the behavior of

equation 24, for the stable region as shown in figure 12, is shown in figure 13. A number of interesting observations concerning the predicted behavior are apparent. First, the calculations indicate that high ratios of maximum acoustic admittance to burning rate pressure exponent occur when $(\beta - \Gamma \Lambda)/\psi$ is negative; that is when the summation of all surface pyrolysis reactions results in a net exothermic process. Under these conditions, the surface pyrolysis reactions which occur at the point of maximum temperature oscillations become sources of energy which amplify the temperature oscillations rather than sinks which attenuate the oscillations. The only source of thermal damping results from the conduction of energy into the solid phase; as a result, the acoustic response function is greatly increased.

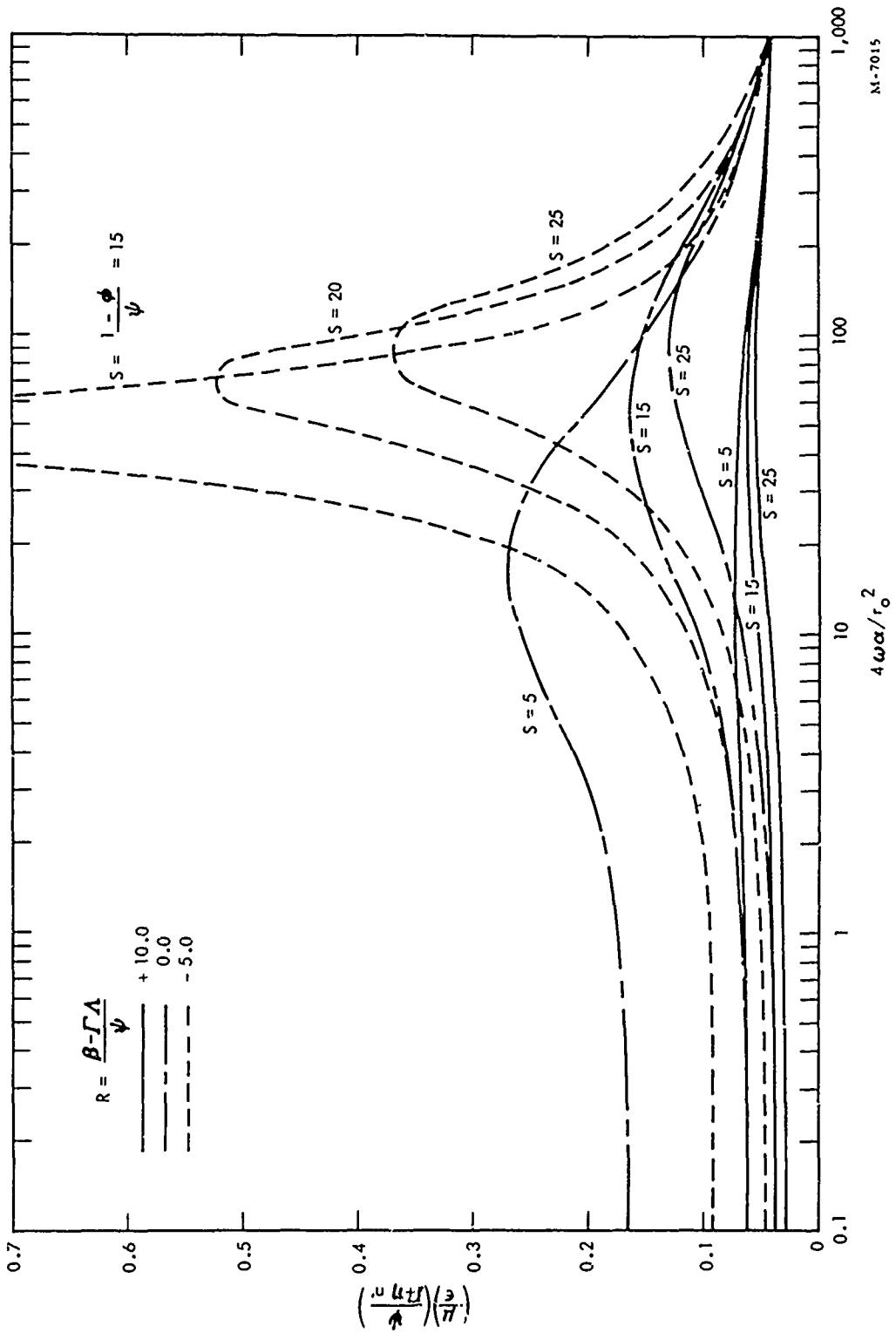


Figure 13. General Response of Linear Model

Another result from the analysis is that the frequency at which the maximum admittance occurs depends only on the temperature parameter, S . This is apparent both by differentiation of equation 20 with respect to λ and from the parametric calculations shown in figure 13. Hence a shift in the frequency at which the maximum response function is observed can only be effected by a change in S .

It should be noted that all the conditions shown in figure 8 are stable in the self-excited modes. Therefore, a propellant can be stable in the self-excited modes but be highly unstable in the combustion chamber as a result of the feedback process between the dynamic pressure response of the combustion chamber to burning rate oscillations.

A third observation concerns the effect of pressure-sensitive surface reactions on the predicted behavior. From figure 13 it is apparent that increasing the contribution of these reactions (i.e., increasing Γ) significantly increases the predicted response function. This then raises the question as to the influence of pressure on the predicted behavior. The calculations shown in figure 13 do not permit the investigation of the pressure effect directly since these calculations were performed by holding the parameters ψ , β , and ϕ constant, which in effect requires that \dot{r}_0 and $T^{\circ}(0)$ remain constant with changing P . However, changes in pressure will obviously change both \dot{r}_0 and $T^{\circ}(0)$. To circumvent this difficulty, the dimensionless groups can be redefined to eliminate the surface temperature as follows:

$$A \equiv \frac{Z_1 P R}{Z_2 C_p E_2} = \psi \Gamma \exp\left(\frac{\Lambda-1}{\psi}\right) \quad (27)$$

$$B \equiv \frac{F R}{Z_2 C_p E_2} = \eta \psi e^{-1/\psi}$$

$$C \equiv RT_{\omega}/E_2 = \psi \phi$$

$$D \equiv \Delta H_v R / C_p E_2 = \psi \beta$$

$$\Lambda \equiv E_1 / E_2$$

Substituting these definitions into the steady-state energy balance (equation 5 written for steady-state conditions)

$$B \exp(1/\psi) + A \exp(1-\Lambda)/\psi = \psi + D - C \quad (28)$$

Thereby, the value for the dimensionless surface temperature can be calculated for each specific set of values for A, B, C, D, and Λ from equation 28. Because parameters A and B are directly related to pressure, the effect of pressure on the theoretical acoustic admittance can be studied using equations 24, 27, and 28. The results are shown in figure 14 for one particular case where surface reactions contribute approximately 20% of the total energy flux to the solid surface. It should be noted that the dimensionless frequency $4\alpha\omega/\dot{x}_0^2 Z_2$ contains the burning rate at the pressure of interest and hence contains a pressure effect which is not apparent in figure 14. To remove the effect, the frequency has been renormalized with respect to Z_2 instead of \dot{x}_0 . Thus, the modified dimensionless frequency becomes

$$\lambda' = 4\alpha\omega/Z_2^2, \quad (29)$$

and is directly proportional to the dimensional frequency ω . On this basis, the results shown in figure 14 have been replotted and are shown in figures 15 and 16.

From figures 14 through 16, it is apparent that the model predicts the frequency at which the maximum acoustic response increases with increasing pressure. This results from the pressure effect on the burning rate and the resultant effect on the characteristic time of heat conduction. This effect should be universal to all combustion models. These figures also show the maximum admittance and pressure exponent increase as the pressure increases. The magnitude of all these effects depend on the values of the various combustion parameters, and further parameter studies are required to determine which parameters are the most significant. These studies are currently in progress.

2.2.3 Comparison of Experiment and Theory in the Linear Region

When the theoretical calculations are considered in the light of experimental observations, some interesting correspondence and some disturbing differences can be noted. First, if the analysis does approximately model the actual combustion process, then the high ratios of the maximum acoustic response function to the pressure exponent of the burning rate signify the net surface pyrolysis processes are either thermally neutral or are exothermic, i.e., R is zero or negative. Unless this is the case, the model cannot account for the $\text{Re } (\mu/\epsilon)_{\text{max}}/n$ values of 4 to 7 which are observed experimentally. This would suggest the exothermic decomposition of ammonium perchlorate plays an important role. This observation is at least consistent with the theoretical calculations of Hermance^(26,27) and with the experimental data obtained by Woesche et al.⁽²⁸⁾

If R is negative, the shift in frequency at which the maximum response occurs when coated oxidizer is used suggests the coatings reduce S by reducing the overall activation energy of the surface pyrolysis reactions or increase $T^\circ(0)$. A reduction in E_2 reduces both the parameters R and S.

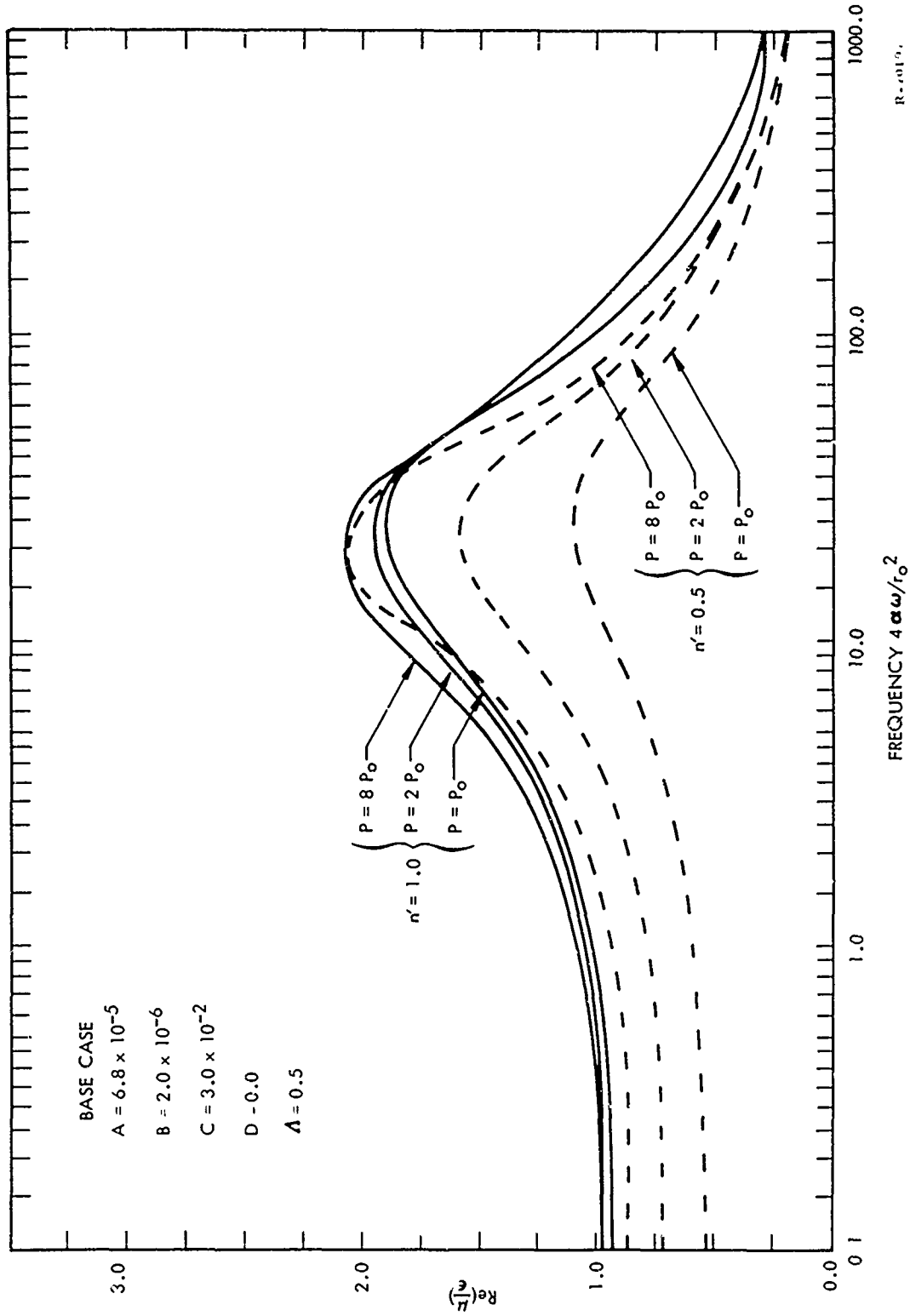


Figure 14. Acoustic Response Function - Moderate Surface Reaction Term Effect on Pressure

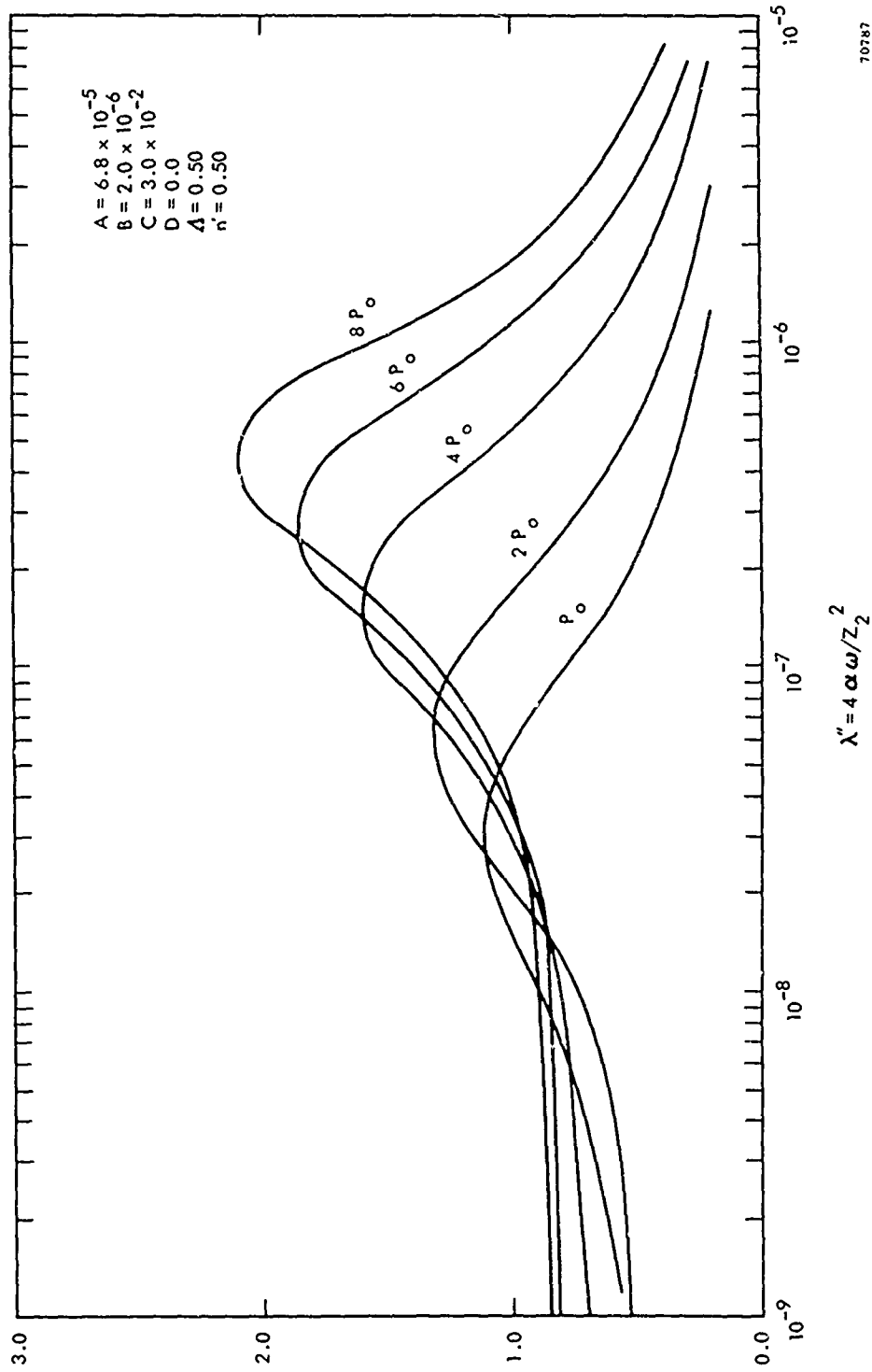


Figure 15. Predicted Acoustic Response for $n'=0.50$ as a Function of λ'

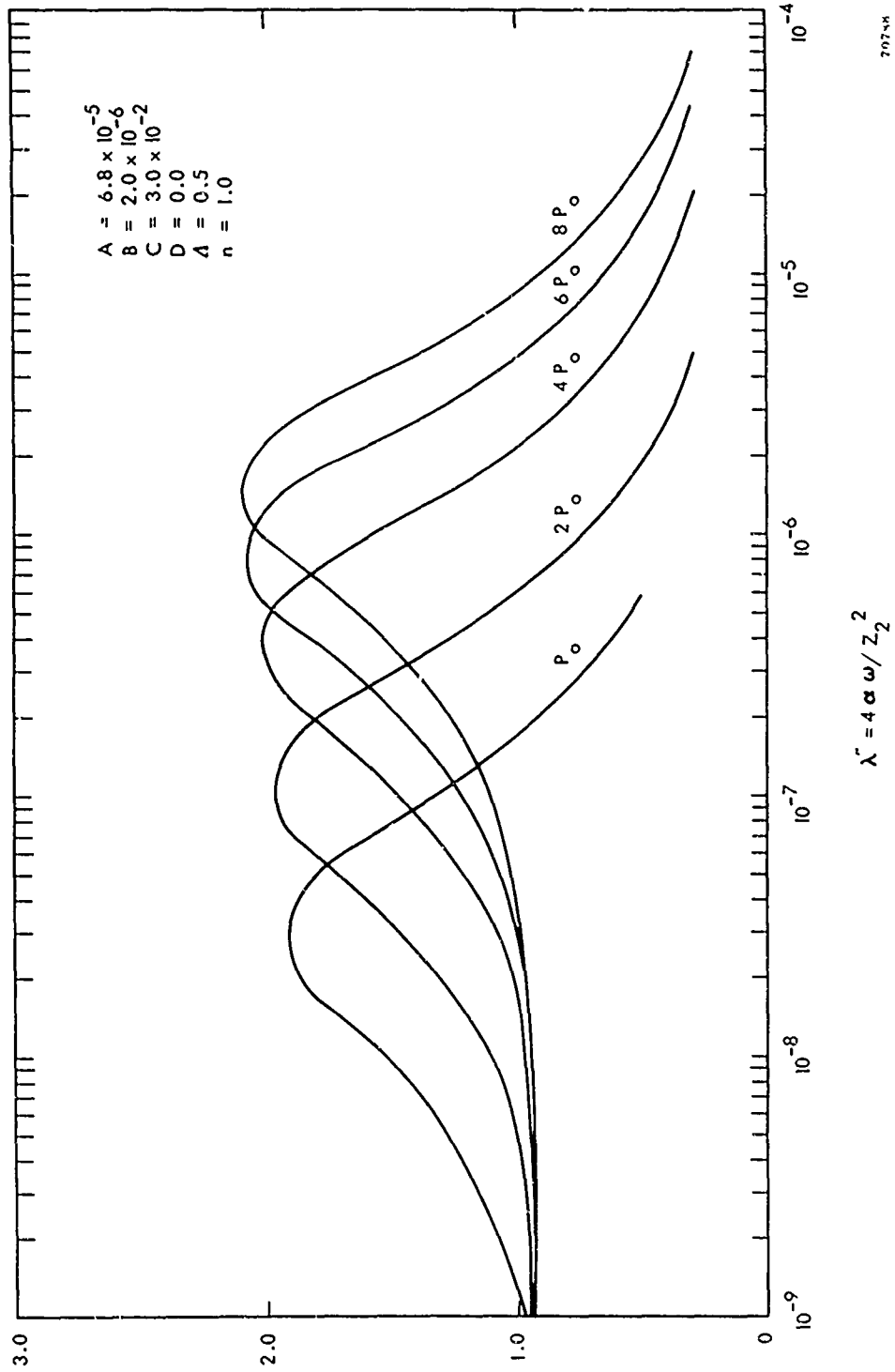


Figure 16. Predicted Acoustic Response for n=1.0 as a Function of λ'

If R is then negative, figure 13 indicates that both the maximum response function and the frequency at which this maximum occurs are reduced. This behavior was observed experimentally with the Kel-F and Viton A coated oxidizer.

However, the effect of other coatings was to shift the maximum response frequency but to not change the maximum response itself. In the context of the analysis, such behavior can only result from a compound effect such as a concurrent decrease in E_2 and an increase in either η , n' , or Γ . The changes in the chemistry which effect this change are not apparent, however. Clearly changing the activation energy suggests a shift in the contribution of the various reactions. One might then expect a concurrent shift in burning rate and surface temperature, but these secondary changes are not apparent from the analysis. More analysis of the results shown in figure 13 are required to elucidate the changes produced by the coatings within the context of the model.

The predicted effect of pressure shown in figure 14 is consistent with experimental observations of Ibiricu⁽²²⁾ and suggest that pressure-dependent surface reactions cannot be a major contribution to the overall combustion process, at least at low pressures for this propellant. Under conditions of even moderate pressure-dependent reactions at the surface, the predicted burning rate pressure exponent increases with increasing pressure. The predicted effect contrasts experimental burning rate data for the propellants studied and thereby raises the question of the validity of the basic model. It should be noted that pressure exponents are generally observed to increase significantly at elevated pressure, i.e., 2000 to 5000 psi for many composite propellants.

The predicted effect of pressure on the acoustic response function shown in figures 13 through 16 has some similarity with the data reported in figures 5 and 6 and with the experimental observations of Ibiricu.⁽²²⁾ Both the magnitude of the maximum acoustic response functions and the frequency at which the maximum occurs increase with increasing pressure at lower pressures. However, there are some serious differences between theory and experiment. At higher pressures the maximum response function continues to increase with pressure while Ibiricu's data show the reverse effect. Furthermore, the predicted shift in the frequency of the maximum response is much larger than observed experimentally. Also the predicted magnitude of the maximum response functions are substantially less than the experimental data. This indicates that the combustion parameters chosen for the parametric study are not characteristics of the propellants studied. The studies currently in progress are directed towards determining the approximate combustion parameters for these various propellants to establish if realistic comparisons between theory and experiment are possible.

2.2.4 Nonlinear Response Studies

Nonlinear analytical studies have been directed toward two aspects of the acoustical behavior: (1) the effect of subsurface reactions and (2) the effect of second order effects in the absence of subsurface reactions.

In the first technical summary report, ⁽¹⁹⁾ the equations describing the effects of subsurface reactions were developed together with the finite difference algorithm for their numerical solution on the digital computer. This development is also presented in appendix B.

Both the computer code for predicting the steady-state temperature distribution within the solid and the code to predict transient behavior have been developed and successfully tested. Good numerical stability and convergence were demonstrated.

However, difficulty arises when the results from the steady-state code are incorporated into the transient analysis. Unfortunately, the calculated profile is never precisely equal to the exact steady-state profile because infinite computer time would be required. The transient analysis considers these errors as heat fluxes from some unknown source or sources. These numerically-generated fluxes are, of course, erroneous but unfortunately they are approximately of equal magnitude with the transient fluxes generated by the oscillating pressure. The calculations conducted to date have shown that these errors cause severe convergence problems. The only apparent method to circumvent this problem is to use similar mesh spacings in both the space and time variables. However, because the computer costs become prohibitive when the required mesh spacings are used, further studies along this avenue were terminated.

The principal justification for using numerical techniques was that subsurface reaction effects on both the linear and nonlinear behavior could be determined. If these effects are assumed to be small, then analytical techniques can be used as an alternate method to estimate the nonlinear behavior of the combustion model. To apply this approach, temperatures within the solid and pressure were expanded in the form

$$P = P_0 \left[1 + \epsilon' \epsilon_1 \exp \left(\frac{i\lambda\tau}{4} \right) + \epsilon'^2 \epsilon_2 \exp \left(\frac{i\lambda\tau}{2} \right) \right] \quad (30)$$

$$T(x,t) = \left[T(x,0) + \epsilon' \theta_1(x,t) + \epsilon'^2 \theta_2(x,t) \right] \quad (31)$$

$$\dot{r}(t) = \dot{r}_0 \left[1 + \frac{\epsilon' \theta_1(0,t) E_2}{RT^2(0,0)} + \frac{\epsilon'^2}{2} \left(\frac{E_2 \theta_1(0,t)}{RT^2(0,0)} \right)^2 + \frac{\epsilon'^2 \theta_2(0,t) E_2}{RT^2(0,0)} \right] \quad (32)$$

Equations 30, 31, and 32 were then substituted into equations 5 and 8 through 11 and collecting terms of the order ϵ'^2 yields

$$\frac{\partial \theta_2}{\partial \tau} = \frac{\partial^2 \theta_2}{\partial \zeta^2} + \frac{\partial \theta_2}{\partial \zeta} + \left\{ \frac{\theta_2(0,t)}{\psi T(0,0)} + \frac{1}{2} \left[\frac{\theta_1(0,t)}{\psi T(0,0)} \right]^2 \right\} \frac{dT(x,0)}{d\zeta} + \frac{\theta_1(0,t)}{\psi T(0,0)} + \frac{\partial \theta_1(0,t)}{\partial \zeta} \quad (33)$$

at $\zeta = 0$

$$\begin{aligned} \frac{-\partial \theta_2(x,t)/T(0,0)}{\partial \zeta} &= (\eta n^1 + \Gamma) \epsilon_2(\tau) + \frac{(\Gamma \Lambda - \beta)}{4T(0,0)} + \frac{(\Gamma \Lambda^2 - \beta)}{2} \left[\frac{\theta_1(0,t)}{\psi T(0,0)} \right]^2 \\ &+ \frac{\eta n^1 (n^1 - 1)}{2} \epsilon_1^2(\tau) + \frac{\Gamma \Lambda \theta_1(0,t) \epsilon_1(\tau)}{\psi T(0,0)} \end{aligned} \quad (34)$$

As $\zeta \rightarrow \infty$ $\theta_2 \rightarrow 0$ (35)

Friedly⁽¹⁴⁾ has noted that the real components in the nonhomogeneous terms, such as $\theta_1^2(0,0)$ should be products of the real components. In other words, these cross products must be regarded as $\text{Re}(\theta_1) \cdot \text{Re}(\theta_1)$ when the complex notation is considered. This observation then leads to the conclusion that these nonhomogeneous terms have the form

$$\text{Re}(x_1) \cdot \text{Re}(x_2) = x_{12}^0(\zeta) + x_{12}^t(\zeta) \exp(i\lambda\tau/2) \quad (36)$$

and hence θ_2 must have the form

$$\theta_2(\zeta) = \theta_2^0(\zeta) + \theta_2^t(\zeta) \exp(i\lambda\tau/2) \quad (37)$$

Thus, consideration of second order effects leads to two solutions, one which is independent of time and one which oscillates at the second harmonic frequency. The time-independent solution represents a shift from the steady state and, therefore, is the more important second order effect.

Substituting equation 36 and 37 into equations 33 and 34 and solving for the time-independent component yields

$$\begin{aligned} &\frac{d^2 \mu_2^0(\zeta)}{d\zeta^2} + \frac{d \mu_2^0(\zeta)}{d\zeta} - S \left\{ \mu_2^0(0) + \left[\frac{\text{Re}^2(\mu/\epsilon) + \text{Im}^2(\mu/\epsilon)}{4} \right] \right\} \\ &+ \frac{\text{Re}^2(\mu/\epsilon) + \text{Im}^2(\mu/\epsilon)}{4} \cdot \left\{ E^1 \cos(M_1 \zeta) - F^1 \sin(M_1 \zeta) \right\} \exp(M_r \zeta) = 0 \end{aligned} \quad (38)$$

$$\begin{aligned} \frac{-d\mu_2^0}{d\zeta} = & T \epsilon_2^0 - R \mu_2^0(0) - \frac{\beta - \Gamma \Lambda^2}{\psi} \left\{ \frac{\text{Re}^2(\mu/\epsilon) + \text{Im}^2(\mu/\epsilon)}{4} \right\} + \frac{\eta n' (n' - 1) \epsilon_1^2}{4 \psi} \\ & + \frac{\Gamma \Lambda}{2\psi} \epsilon_1^2 \text{Re}(\mu/\epsilon) \end{aligned} \quad (39)$$

where

$$\begin{aligned} E^1 &= M_r + 4S M_i / \lambda \\ F^1 &= M_i - 4S M_r / \lambda \\ M_r &= - \left\{ 1 + (1 + \lambda^2)^{1/4} \cos \nu \right\} / 2 \\ M_i &= - \left\{ (1 + \lambda^2)^{1/4} \sin \nu \right\} / 2 \\ \nu &= 0.5 \tan^{-1}(\lambda) \end{aligned}$$

$$\mu_2^0(\zeta) \rightarrow 0 \text{ as } \zeta \rightarrow \infty$$

Solving equations 38, 39, and 40 and assuming no change in the steady-state pressure (i.e., $\epsilon_2 = 0$) yields

$$\begin{aligned} \frac{\mu_2^0}{\epsilon_1^2} = & \left[\left\{ \frac{\text{Re}^2(\mu/\epsilon) + \text{Im}^2(\mu/\epsilon)}{2} \right\} \left\{ \frac{M_i (FB' - EA') - (1 + M_r) (A'F + B'E)}{(A')^2 + (B')^2} \right\} - \frac{S}{2} - \frac{(\beta - \Gamma \Lambda^2)}{2\psi} \right] \\ & + \frac{\eta n' (n' - 1)}{4\psi} + \frac{\Gamma \Lambda}{2\psi} \text{Re}(\mu/\epsilon) \Bigg] / (1 + R + S) \end{aligned} \quad (41)$$

where

$$A' = M_i (1 + 2M_r) \quad (42)$$

$$B' = M_r^2 - M_i^2 + M_r \quad (43)$$

Substituting equation 41 and 24 into equation 32 therefore permits the change in burning rate, i.e.,

$$\frac{\Delta \dot{r}}{\dot{r}_0} = \left\{ \frac{\mu^0}{\epsilon_1^2} + \frac{\text{Re}^2(\mu/\epsilon) + \text{Im}^2(\mu/\epsilon)}{4.0} \right\} \epsilon_1^2$$

The results of parametric studies conducted to date are shown in figures 17 and 18 for the same cases shown in figures 14 through 16. In figure 17, the effect of increasingly exothermic pyrolysis reactions is seen to increase the magnitude of the shift in steady-state burning rate. Comparing the results on figure 14 with those on figure 17 shows the maximum acoustic response and the maximum decrease in burning rate both occur at the same frequency.

It should be noted that the maximum change shown in figure 17 still represents a small shift in burning rate. Typical values for ϵ_1 , in the T-burner are 0.1 to 0.3 and hence the maximum decrease in burning rate shown in figure 16 is approximately 2%. This value is of the same order of magnitude as the experimental observations of Eisel.⁽³⁰⁾ Since there is no assurance that the constant parametric values used to prepare Figure 16 are characteristic of Eisel's propellants, the differences between theory and experiment have no significance.

Figure 18 shows the predicted effect of pressure on the burning rate changes, again for the same basic set of parameters used in figures 14 through 16. Two results are of particular interest. First, there appears to be little effect of pressure on the shift in burning rate. This holds for both the case where $n'=1.0$ as shown and for the case of $n'=0.5$. In view of the larger pressure effect on the maximum acoustic response function when $n'=0.5$, it appears that the second order pressure effect is generally small. However, this should be taken as a preliminary observation since a wide range of combustion parameters have not been considered.

The second result shown in figure 18 is the very small increase in burning rate at the lower frequencies under oscillating pressure conditions. This result is real when the limits of equation 44, 41, and 24 are considered and results from the particular set of combustion parameters chosen for study. This effect appears to be extremely small in any event and is therefore more of a theoretical curiosity than of a practical interest.

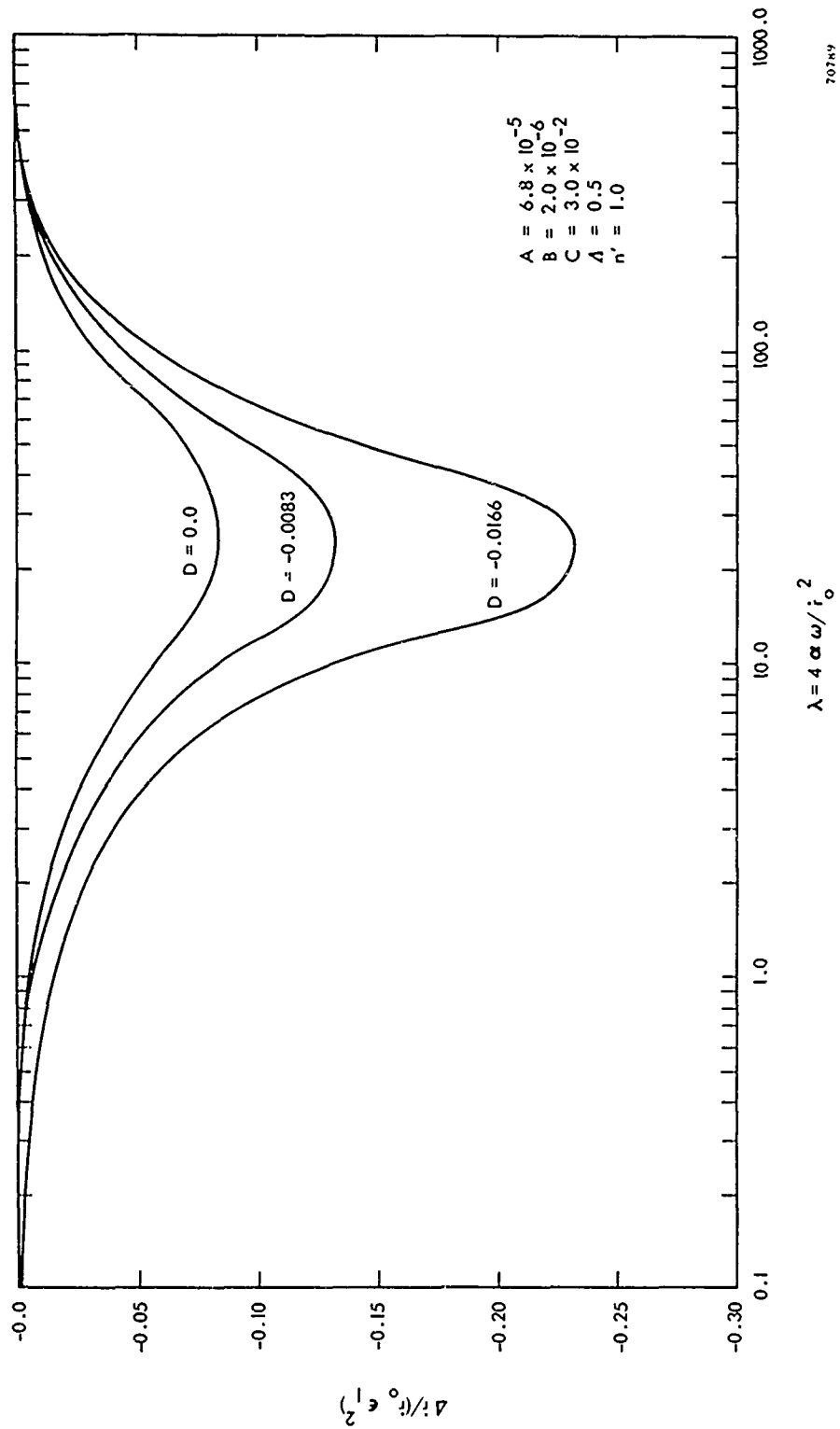
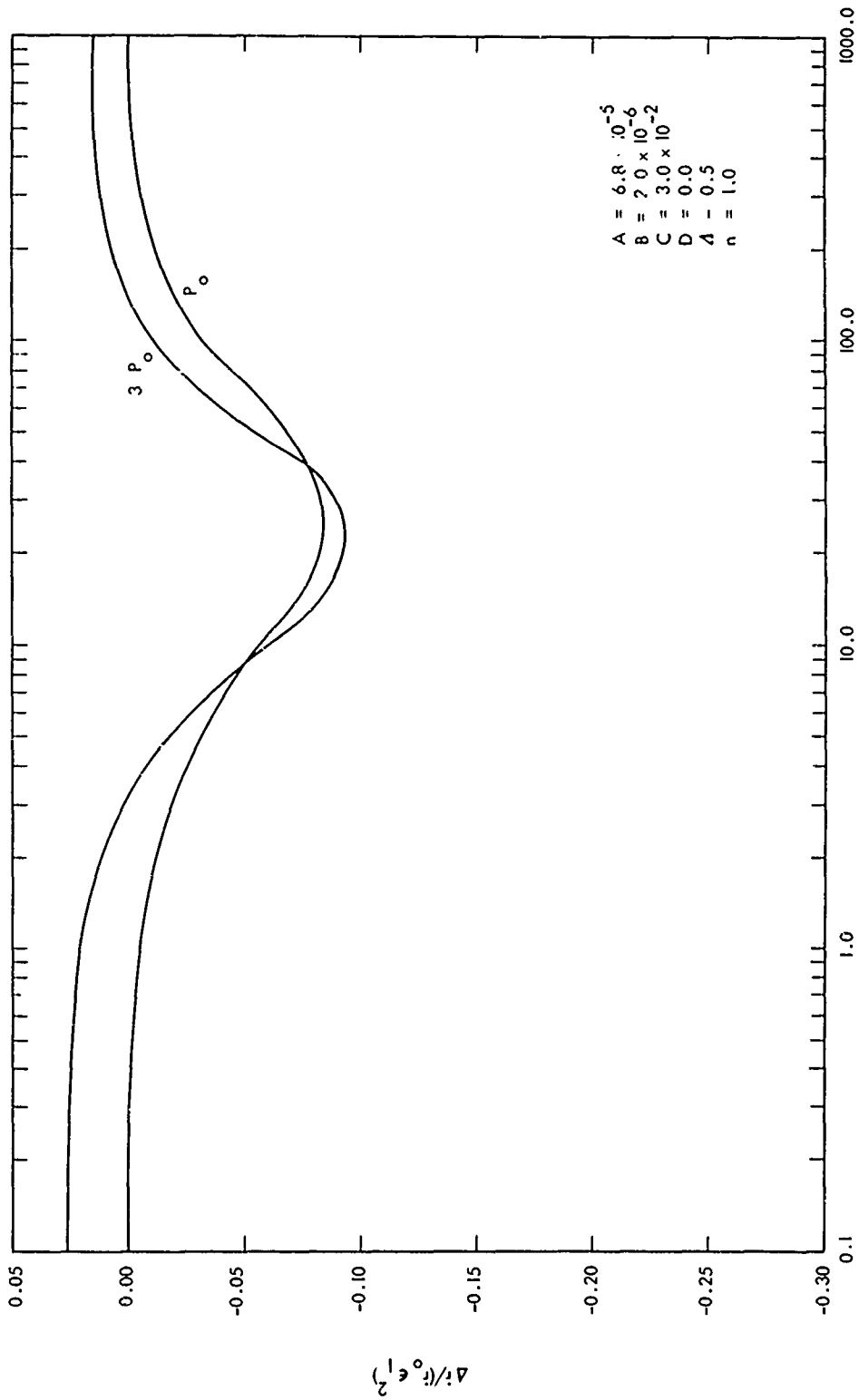


Figure 17. Effect of D on Predicted Shift in Burning Rate



$$\lambda = 4 \alpha \omega / r_0^2$$

Figure 18. Effect of Pressure on Predicted Shift in Burning Rate

REFERENCES

1. Wenograd, J., "Solid Propellant Combustion Studies," Tenth Symposium (International) on Combustion, The Combustion Institute, Pittsburgh, Pennsylvania, 1965, pp. 1379.
2. Most, W. J., and J. Wenograd, "Solid Propellant Combustion Mechanism Studies," Seventeenth Progress Report, Contract No. Nor 1858(32), Princeton University, June 1965.
3. Steinz, J. A., and M. Summerfield, "Solid Propellant Combustion Mechanism Studies," Eighteenth Progress Report, Contract No. Nor 1858(32) Princeton University, July 1965.
4. Anderson, R., R. S. Brown, G. T. Thompson, and R. W. Ebeling, "Theory of Hypergolic Ignition of Solid Propellants," AIAA Preprint 63-514, December 1963.
5. Anderson, R., and R. S. Brown, "The Structure of the Combustion Zone in Composite Solid Propellant Burning, Termination and Instability," presented at 2nd ICRPG Combustion Conference, Orlando, Florida, November 1964.
6. Brown, R. S., and R. Anderson, "Pressure Coupling with Chemical Mechanism of the Combustion Zone of Composite Solid Propellant Burning," presented at 2nd ICRPG Combustion Conference, Orlando, Florida, November 1964.
7. Summerfield, M., G. S. Sutherland, M. J. Webb, H. J. Tabach, and K. P. Hall, "Burning Mechanism of Ammonium Perchlorate Propellants," Advances in Astronautics and Aeronautics, Vol. 1, New York: Academic Press, 1960. pp. 141-182.
8. Nachbar, W., "A Theoretical Study of the Burning of a Solid-Propellant Sandwich," Advances in Astronautics and Aeronautics, Vol. 1, New York: Academic Press, 1960. pp. 207-226.
9. Rosen, G., "Burning Rates of Solid Propellants," J. Chem. Phys., Vol. 32: 1, 1960. pp. 89-93.
10. Spaulding, D. B., "The Theory of Burning of Solid and Liquid Propellants," Combustion and Flame, Vol. 4: 1, 1960. pp. 59-76.
11. McClure, F. T., R. W. Hart, and J. F. Bird, "Solid Propellant Rocket Motors as Acoustic Oscillators," Advances in Astronautics and Rocketry, Vol. 1, New York: Academic Press, 1960. pp. 295-358.

12. Williams, F. A., "Response of a Burning Solid to Small-Amplitude Pressure Oscillations," Journal of App. Physics, Vol. 33: 11, 1962. pp. 3153-3166.
13. Friedly, J. C., and E. E. Peterson, "The Influence of Combustion Parameters on Instability in Solid Propellant Motors: Part I Development of Model and Linear Analysis," AIAA Journal, Vol. 4: 9, 1966. pp. 1604-1610.
14. Friedly, J. C., and E. E. Peterson, "Influence of Combustion Parameters on Instability in Solid Propellant Motors: Part II; Nonlinear Analysis," AIAA Journal, Vol. 4:11, 1966. pp. 1932-1937.
15. Friedly, J. C., and E. E. Peterson, "A Mathematical Analysis of the Nonlinear Dynamics of Solid Propellant Combustion: An Application of the Method of Discretization," presented at the International Control Conference, London, June 1966.
16. Capener, E. L., L. A. Dickinson, and G. A. Marxman, "Propellant Combustion Phenomenon During Rapid Depressurization," Quarterly Report No. 1, Contract NAS 7-389, Stanford Research Institute, October 1965.
17. Horton, M. D., "Testing the Dynamic Stability of Solid Propellants: Techniques and Data," Report NOTS TP 3610. U.S. Naval Ordnance Test Station, August 1964.
18. Strittmater, R., L. Watermeier, and S. Pfaff, "Virtual Specific Acoustic Admittance Measurements of Burning Solid Propellant Surface by a Resonant Tube Technique," Ninth Symposium (International) on Combustion, Academic Press, New York, 1963, pp. 311-315.
19. Brown, R. S., R. J. Muzzy, and M. E. Steinle, "Research on Combustion of Solid Propellants," Technical Summary Report No. 1, Contract DA-04-200-AMC-968(X). United Technology Center, July 1966.
20. Coates, R. L., N. W. Ryan, and M. D. Horton, "The T-Burner Method for Determining the Acoustic Admittance of Burning Propellants," AIAA Preprint No. 64-137, January 1964.
21. Horton, M. D. and D. W. Rice, "The Effects of Compositional Variables Upon Oscillatory Combustion of Solid Rocket Propellants," Combustion and Flame, Vol. 8: 1, 1964. pp. 21-28.
22. Ibiricu, M. M., "Results in Pressure-Coupled Instability," presented at the 2nd ICRPG Combustion Conference, Orlando, Florida, November 1964.
23. Penner, S. S., Chemical Rocket Propulsion and Combustion Research, New York: Gordon and Beech, 1962. pp. 126-139.

24. Marxman, G. A., and C. E. Wooldridge, "The Effect of Surface Reactions on the Solid Propellant Response Function," presented at the ICRPG/AIAA 2nd Solid Propulsion Conference, Anaheim, California, June 1967.
25. Denison, M. R., and E. Baum, "A Simplified Model of Unstable Burning in Solid Propellants," ARS Journal, Vol. 31: 8, 1961. pp. 1112-1121.
26. Hermance, E. C., "A Detailed Model of the Combustion of Composite Solid Rockets," presented at the ICRPG/AIAA 2nd Solid Propulsion Conference, Anaheim, California, June 1967.
27. Hermance, C. E., "A Model of Composite Propellant Combustion Including Surface Heterogeneity and Heat Generation," AIAA Journal, Vol. 4: 9, 1966. pp. 1629-1637.
28. Baer, A. D., "Ignition of Solid Propellants," presented at the 20th CPIA Meeting, Ignition Specialists Session, Philadelphia, Pennsylvania, July 1964.
29. Waesche, R. H. W., J. Wenograd, and L. R. Feinauer, "Investigation of Solid Propellant Decomposition Characteristics and their Relation to Observed Burning Rate," presented at ICRPG/AIAA 2nd Propulsion Conference, Anaheim, California, June 1967.
30. Eisel, J. L., "The Effect of Acoustic Pressure on the Burning Rates of Solid Rocket Propellants," Pyrodynamics, Vol. 1: 1, 1964. pp 61-70.

APPENDIX A

EXPERIMENTAL DATA

Data for the propellants tested on the present program are tabulated in this appendix. In addition, the acoustic response data are shown as a function of the measured growth frequency. Previously reported results⁽¹⁹⁾ were made using a frequency based on $8\pi f_g / r_o^2$. This latter form was suggested by the theoretical studies.

Propellant: UTX-8501 (78% AP - 190 μ 3 CT-3 Binder)

Propellant density: 0.063 lbs/in³

Velocity of sound in product gas (c): 36,500 m/sec.

Run No.	Mean Pressure	Growth Frequency	Growth Rate, α_g	Decay Frequency	Decay Rate, α_d	Re(μ/ϵ)
1	200 psig	151	4.72	151	2.27	3.72
2		160	4.24	144	3.11	3.85
3		228	9.92	292	3.48	4.96
4		239	10.20	266	2.92	4.31
5		400	13.97	219	7.76	5.54
6		307	18.81	285	2.83	5.72
7		477	27.40	785	5.13	5.15
8		500	28.55	741	7.21	5.37
9		816	18.77	579	11.56	3.37
10		784	18.92	615	10.52	3.26
11		816	8.98	563	15.68	3.13
12		1904	13.61	1818	6.33	0.85
13		1812	13.29	1904	10.04	1.02
14		2105	10.34	1904	4.33	0.57

Propellant: MTX 8501

Propellant density: 0.063 lbs/in^3

Velocity of sound in product gas (c):

Run No.	Mean Pressure	Growth Frequency	Growth Rate, α_g	Decay Frequency	Decay Rate, α_d	$Re(\omega/c)$
1	100 psig	163	3.76	180	4.48	2.38
2		137	4.03	184	7.76	3.54
3		167	6.18	193	9.86	3.13
4		195	2.35	205	11.90	3.49
5		333	5.30	320	1.01	0.95
6		327	5.88	296	0.97	1.05
7		320	4.53	291	2.24	1.08
8		728	2.20	667	1.72	0.29
9		762	2.16	762	2.60	0.31
10		728	1.81	695	2.33	0.29

Propellant: UTX 8501

Propellant density: 0.063 lbs/in³

Velocity of sound in product gas (c):

Run No.	Mean Pressure	Growth Frequency	Growth Rate, α_g	Decay Frequency	Decay Rate, α_d	Re(μ/ϵ)
1	500 psig	140	296	164	4.76	5.20
2	}	186	3.57	126	2.37	3.95
3		177	1.97	166	4.29	3.51
4		226	9.78	216	4.78	6.75
5		220	10.88	242	5.16	7.32
6		260	12.80	270	8.90	8.33
7		762	7.14	728	17.90	3.52
8		667	5.00	762	25.10	4.17
9		800	5.30	762	34.70	5.90

Propellant: *UTX-8502 (78% AP coated with 1.5% KCl-F
 0 CT-3 Binder)*

Propellant density: *0.063 lbs/m³*

Velocity of sound in product gas (c): *34,000 in/sec.*

Run No.	Mean Pressure	Growth Frequency	Growth Rate, α_g	Decay Frequency	Decay Rate, α_d	Re(μ/ϵ)
1	<i>20 psia</i>	190	5.50	164	2.23	3.55
2	}	188	2.69	161	4.72	3.65
3		168	3.94	160	3.20	3.63
4		271	4.08	313	7.41	3.23
5		307	4.56	290	7.18	3.30
6		242	4.95	313	5.94	3.28
7		667	4.99	635	3.57	1.04
8		513	6.77	769	1.00	1.19

Propellant: *UTX-8525-1 (78% AP (100μ) - CT-3 Binder)*

Propellant density: *0.063 lbs/in³*

Velocity of sound in product gas (c): *36,500 in/sec.*

Run No.	Mean Pressure	Growth Frequency	Growth Rate, α_g	Decay Frequency	Decay Rate, α_d	Re(μ/ϵ)
1	<i>200 psia</i>	<i>146</i>	<i>5.18</i>	<i>131</i>	<i>4.99</i>	<i>4.90</i>
2	}	<i>137</i>	<i>5.00</i>	<i>139</i>	<i>5.46</i>	<i>5.33</i>
3		<i>220</i>	<i>8.79</i>	<i>223</i>	<i>9.60</i>	<i>5.77</i>
4		<i>210</i>	<i>8.93</i>	<i>218</i>	<i>8.06</i>	<i>5.43</i>
5		<i>685</i>	<i>13.47</i>	<i>697</i>	<i>3.43</i>	<i>1.75</i>
6		<i>755</i>	<i>3.21</i>	<i>631</i>	<i>13.38</i>	<i>1.77</i>
7			<i>1620</i>	<i>could not measure a growth curve on several runs</i>		

Propellant: UTX-8526-1 (190 μ AP coated with 1% CAB-O-SIL,
 Propellant density: 0.063 lbs/in³ 1% KE-1-F & CT-3 Binder)
 Velocity of sound in product gas (c): 36,000 in/sec.

Run No.	Mean Pressure	Growth Frequency	Growth Rate, α_g	Decay Frequency	Decay Rate, α_d	Re(μ/ϵ)	
1	200 psig	160	4.51	210	2.35	2.14	
2	}	160	5.11	202	1.98	2.27	
3		280	17.80	285	5.37	4.98	
4		600	16.67	770	7.35	2.04	
5		570	25.88	636	11.74	3.46	
6		1500	could not measure a growth curve on several runs				

Propellant: *UTX-8527-1 (190 μ AP coated with 2% LiF,*

Propellant density: 0.063 lbs/in³ 1% KCLF & CT-3 Binder)

Velocity of sound in product gas (c): 36,000 in/sec.

Run No.	Mean Pressure	Growth Frequency	Growth Rate, α_g	Decay Frequency	Decay Rate, α_d	Re(μ/E)
1	200 psig	120	1.23	165	1.14	2.53
2		123	1.41	170	1.97	3.37
3		231	3.59	275	3.82	4.30
4		216	5.76	263	2.35	5.22
5		700	could not measure a growth curve on several runs			

Propellant: UTX-8528-1 (190 μ AP coated with 1.5% HYPRALON-30
 Propellant density: 0.063 lbs/in³ ° (T-3 Binder)
 Velocity of sound in product gas (c): 36,000 in/sec.

Run No.	Mean Pressure	Growth Frequency	Growth Rate, α_g	Decay Frequency	Decay Rate, α_d	Re(μ/E)	
1	200 psig	166	4.95	146	5.25	4.75	
2	}	127	3.64	193	5.96	5.06	
3		256	9.72	295	2.67	3.52	
4		296	4.28	256	6.77	2.95	
5		600	could not measure a growth curve on several runs				

Propellant: UTX-8529-1 (190 μ AP coated with 1.5% ETHYL-
 Propellant density: 0.063 lbs/in³ CELLULOSE : CT-3 Binder)

Velocity of sound in product gas (c): 36,000 in/sec.

Run No.	Mean Pressure	Growth Frequency	Growth Rate, α_g	Decay Frequency	Decay Rate, α_d	Re(μ/ϵ)	
1	200 psig	174	4.65	176	5.55	3.92	
2	}	163	5.20	161	4.51	4.05	
3		256	15.29	285	4.81	5.16	
4		294	9.79	284	6.47	4.23	
5		525	31.32	730	5.76	4.54	
6		527	32.70	784	6.91	4.76	
7		1690	could not measure a growth curve on several runs				

Propellant: UTX-8531-1 (uncoated with 0.77% CAB-O-SIL)

Propellant density: 0.063 lbs/in³ 0.77% KEL-F in mix

Velocity of sound in product gas (c): 36,000 in/sec

()

Run No.	Mean Pressure	Growth Frequency	Growth Rate, α_g	Decay Frequency	Decay Rate, α_d	Re(μ/ϵ)
1	200 psig	197	3.66	167	5.50	3.38
2		172	4.65	170	7.00	3.98
3		190	9.23	215	9.16	5.33
4		210	8.63	265	9.10	4.92
5		200	7.98	254	13.88	5.39
6		583	31.55	750	5.85	3.62
7		574	32.10	611	12.73	4.87
8		1800	could not measure a growth curve on several runs			

Propellant: *UTX-8532-1 (uncoated with 1.18% Ket-F in mix.)*
 Propellant density: *0.063 lbs/m³*
 Velocity of sound in product gas (c): *36,000 m/sec.*

Run No.	Mean Pressure	Growth Frequency	Growth Rate, α_g	Decay Frequency	Decay Rate, α_d	Re(μ/E)
<i>1</i>	<i>200 psig</i>	<i>165</i>	<i>5.83</i>	<i>135</i>	<i>6.26</i>	<i>6.83</i>
<i>2</i>		<i>175</i>	<i>5.69</i>	<i>136</i>	<i>5.64</i>	<i>6.20</i>
<i>3</i>		<i>233</i>	<i>9.83</i>	<i>232</i>	<i>7.91</i>	<i>6.22</i>
<i>4</i>		<i>490</i>	<i>18.31</i>	<i>755</i>	<i>15.27</i>	<i>4.82</i>
<i>5</i>		<i>475</i>	<i>21.51</i>	<i>690</i>	<i>4.92</i>	<i>4.32</i>
<i>6</i>		<i>1500</i>	<i>3.15</i>	<i>1700</i>	<i>7.11</i>	<i>0.52</i>

Propellant: *ATX-9164 (78% AP coated with 3.0% Kel-F.*
Propellant density: *0.063 lbs/in³ 190µ : CT-3 Binder)*
Velocity of sound in product gas (c): *34,000 in/sec*

Run No.	Mean Pressure	Growth Frequency	Growth Rate, α_g	Decay Frequency	Decay Rate, α_d	Re(μ/ϵ)
1	<i>200 psig</i>	<i>200</i>	<i>1.38</i>	<i>182</i>	<i>4.26</i>	<i>2.56</i>
2		<i>205</i>	<i>2.09</i>	<i>190</i>	<i>3.02</i>	<i>2.27</i>
3		<i>291</i>	<i>10.30</i>	<i>302</i>	<i>3.41</i>	<i>3.95</i>
4		<i>291</i>	<i>7.25</i>	<i>341</i>	<i>2.60</i>	<i>2.85</i>
5		<i>333</i>	<i>1.49</i>	<i>296</i>	<i>9.10</i>	<i>2.98</i>
6		<i>364</i>	<i>4.05</i>	<i>314</i>	<i>9.57</i>	<i>3.81</i>
7		<i>372</i>	<i>3.66</i>	<i>262</i>	<i>9.07</i>	<i>2.20</i>
8		<i>696</i>	<i>4.31</i>	<i>696</i>	<i>2.93</i>	<i>0.84</i>
9		<i>727</i>	<i>1.60</i>	<i>762</i>	<i>2.38</i>	<i>0.97</i>

Propellant: *UTX-9165 (78% AP coated with 1.5% VitonA
 Propellant density: 0.063 lbs/mi³ ; OF-3 Binder)*
 Velocity of sound in product gas (c): *34,000 mi/sec*

Run No.	Mean Pressure	Growth Frequency	Growth Rate, α_g	Decay Frequency	Decay Rate, α_d	Re(μ/E)	
1	<i>200 psig</i>	191	5.11	170	3.06	3.76	
2	}	190	3.66	174	3.09	3.11	
3		174	4.93	174	2.96	3.56	
4		190	4.46	170	3.40	3.66	
5		170	4.62	178	1.83	3.15	
6		320	2.43	250	3.97	1.97	
7	}	320	3.30	222	2.72	1.89	
8		347	3.06	235	3.00	1.81	
9		320	2.23	242	5.09	2.35	
10	}	750	3.24	750	2.56	0.65	

Propellant: *MTX - 9167 (78% AP & PBAN Binder epoxy cure)*

Propellant density: *0.063 lbs/in³*

Velocity of sound in product gas (c): *36,500 in/sec.*

Run No.	Mean Pressure	Growth Frequency	Growth Rate, α_g	Decay Frequency	Decay Rate, α_d	Re(γ_i/ϵ)
<i>1</i>	<i>200 psig</i>	<i>228</i>	<i>3.61</i>	<i>170</i>	<i>2.67</i>	<i>1.98</i>
<i>2</i>		<i>216</i>	<i>3.57</i>	<i>170</i>	<i>2.34</i>	<i>1.90</i>
<i>3</i>		<i>222</i>	<i>4.98</i>	<i>186</i>	<i>1.98</i>	<i>1.94</i>
<i>4</i>		<i>223</i>	<i>3.60</i>	<i>211</i>	<i>3.63</i>	<i>2.10</i>
<i>5</i>		<i>333</i>	<i>7.44</i>	<i>222</i>	<i>3.77</i>	<i>2.46</i>
<i>6</i>		<i>320</i>	<i>4.68</i>	<i>222</i>	<i>6.04</i>	<i>2.70</i>
<i>7</i>		<i>800</i>	<i>3.52</i>	<i>800</i>	<i>6.03</i>	<i>0.75</i>
<i>8</i>		<i>800</i>	<i>3.17</i>	<i>730</i>	<i>6.82</i>	<i>0.84</i>

Propellant: UTX-9168 (78% AP 3 PBAN Binder 33 magp cure)

Propellant density: 0.063 lbs/in³

Velocity of sound in product gas (c): 36,500 in/sec.

Run No.	Mean Pressure	Growth Frequency	Growth Rate, α_g	Decay Frequency	Decay Rate, α_d	Re(μ/ϵ)
1	200 (psig)	200	3.36	163	5.12	3.91
2	}	195	2.96	157	4.65	3.17
3		191	1.69	195	5.93	3.28
4		333	5.32	250	7.15	3.16
5		333	2.52	210	6.15	2.61
6		320	2.65	266	6.52	2.32
7		276	3.24	302	6.93	2.57
8		533	11.95	730	7.02	2.11
9		696	10.20	800	3.50	1.35

Propellant: UTX 9173 (78% AP-CT3 Binder^{ss} epoxy cure)

Propellant density: 0.063 lbs/in³

Velocity of sound in product gas (c): 36,500 in/sec.

Run No.	Mean Pressure	Growth Frequency	Growth Rate, α_g	Decay Frequency	Decay Rate, α_d	Re(α/ϵ)
1	220 psig	210	9.54	200	8.60	5.80
2		210	8.53	200	9.71	5.85
3		216	5.79	160	9.80	5.80
4		381	9.16	398	3.98	2.32
5		381	9.03	398	4.16	2.33
6		360	5.90	276	4.58	2.08
7		382	6.59	260	4.91	2.37
8		800	5.25	806	16.56	1.79
9		552	11.30	893	5.88	1.81

Propellant: UTX 9368 (84% AP $\left\{ \begin{array}{l} 70\% \text{ MS-4}, \\ 30\% \text{ Fines} \end{array} \right\}$;
 Propellant density: $0.063 \text{ lb}_m/\text{in}^3$ (UTREZ binder)
 Velocity of sound in product gas (c): $36,500 \text{ m/sec.}$

Run No.	Mean Pressure	Growth Frequency	Growth Rate, α_g	Decay Frequency	Decay Rate, α_d	Re(μ/ϵ)
1	200psig	239	14.78	267	2.94	5.23
2		220	13.38	267	2.41	5.05
3		239	13.21	276	3.10	4.80
4		372	24.90	762	8.68	5.55
5		400	14.75	727	7.94	4.15
6		533	22.7	800	8.47	3.82
7		1010	6.15	1145	12.40	1.21
8		1080	8.32	1250	15.20	1.43

Propellant: *A-13 (NOTS PROPELLANT)*Propellant density: *0.057 lbs/in³*Velocity of sound in product gas (c): *36,500 in/sec.*

Run No.	Mean Pressure	Growth Frequency	Growth Rate, α_g	Decay Frequency	Decay Rate, α_d	Re(μ/ϵ)
1	<i>200 psig</i>	242	6.4	157	10.3	5.64
2		243	5.4	182	13.2	5.81
3		320	6.5	314	13.5	3.88
4		333	7.2	286	8.6	3.17
5		690	5.2	572	8.7	1.43
6		696	5.5	552	10.4	1.64
7		728	6.9	762	12.3	1.57
8		728	7.1	572	11.1	1.79
9		800	5.2	900	17.5	1.72
10		1430	11.0	1820	20.6	1.16
11		1430	9.5	1504	25.4	1.94
12		1540	14.4	1740	13.2	1.04
13		1670	10.4	1820	29.6	1.21
14		3300	4.3	3330	23.0	0.51
15		3300	9.2	2850	37.3	0.97
16		4000	22.3	4450	5.9	0.92

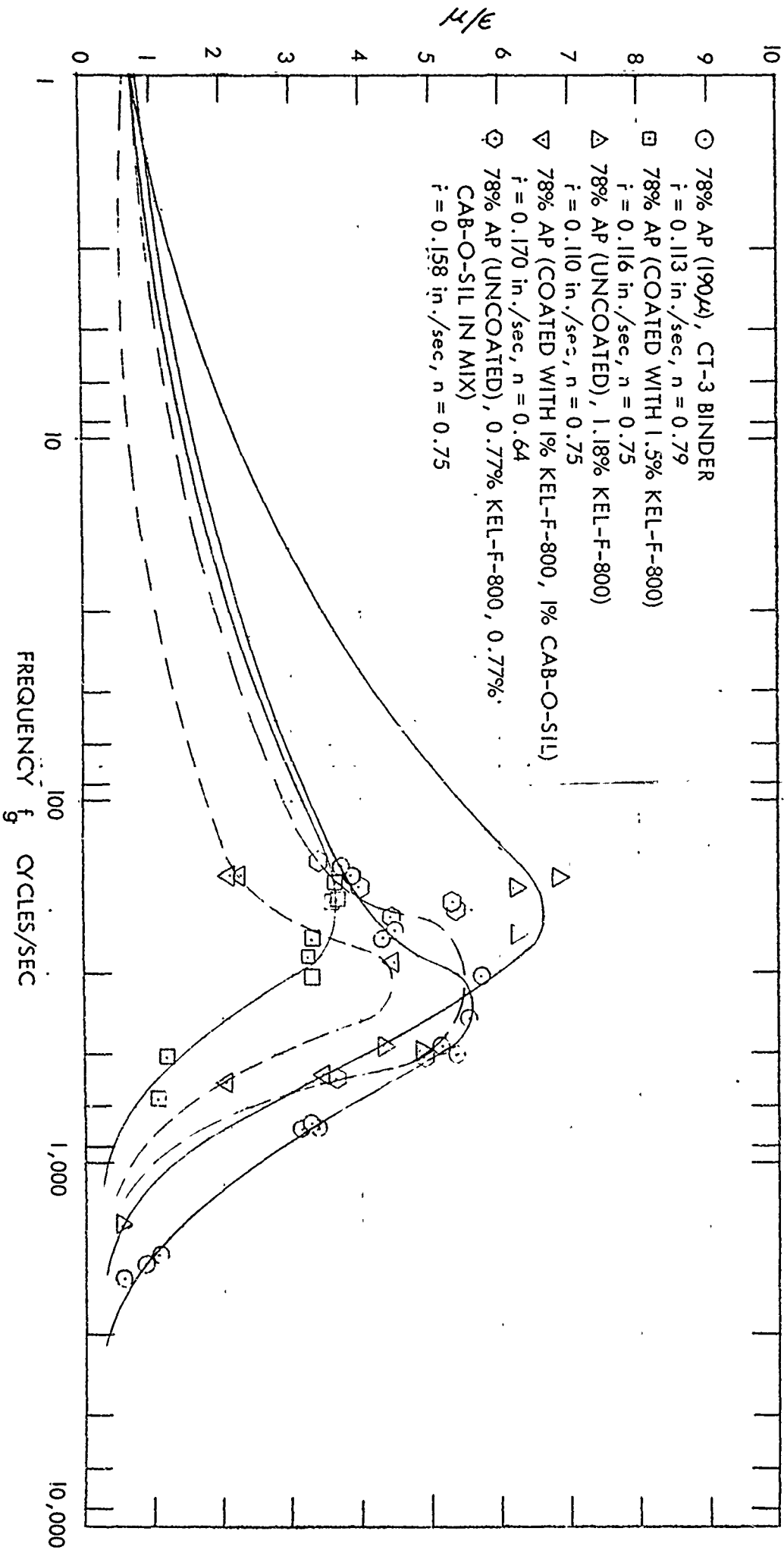


FIGURE 1. EFFECT OF COATING OR ADDITION TO PROPELLANT MIX

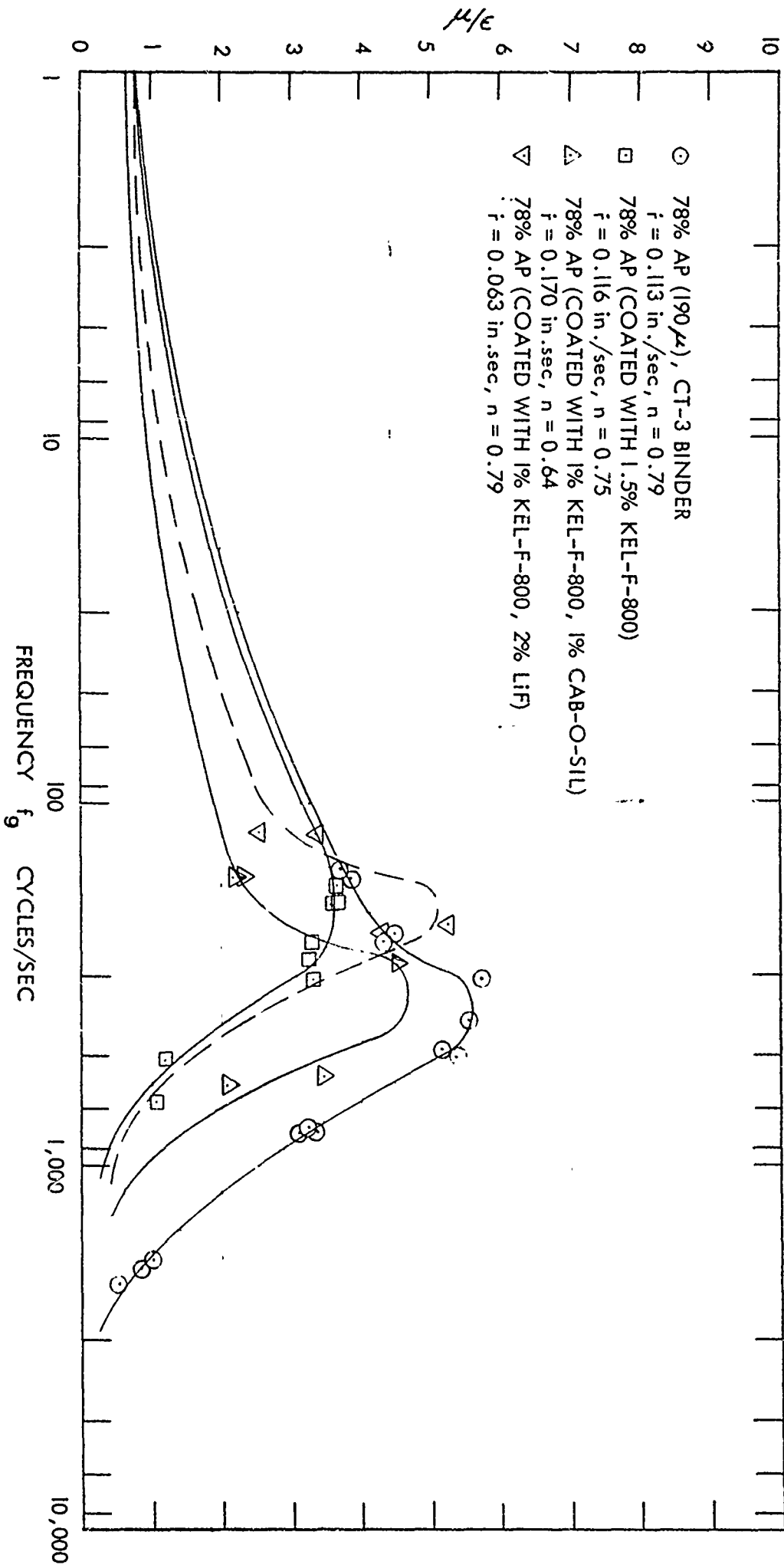


FIGURE 2. EFFECT OF KEL-F COATINGS

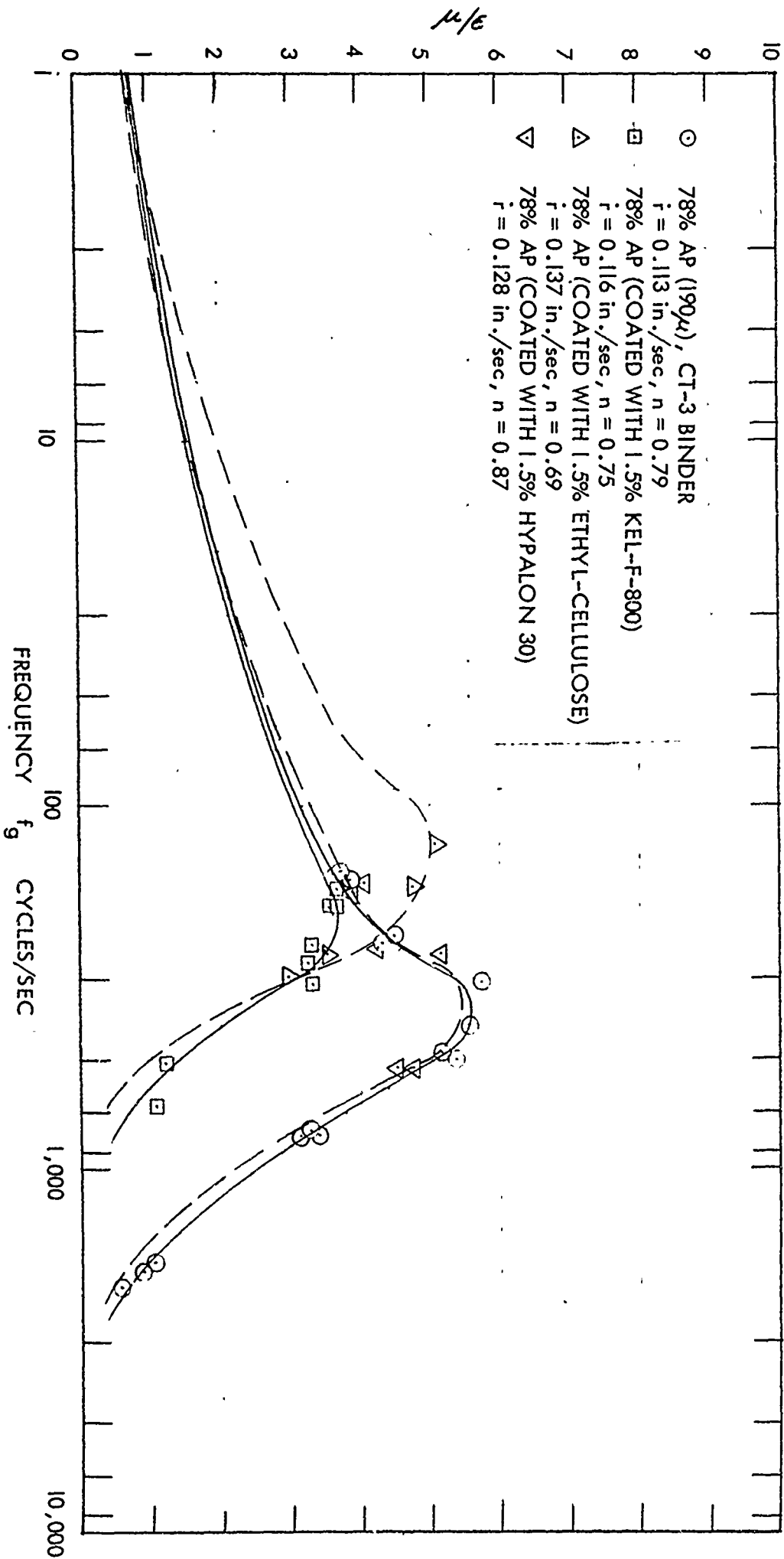


FIGURE 3. EFFECT OF VARIOUS COATINGS

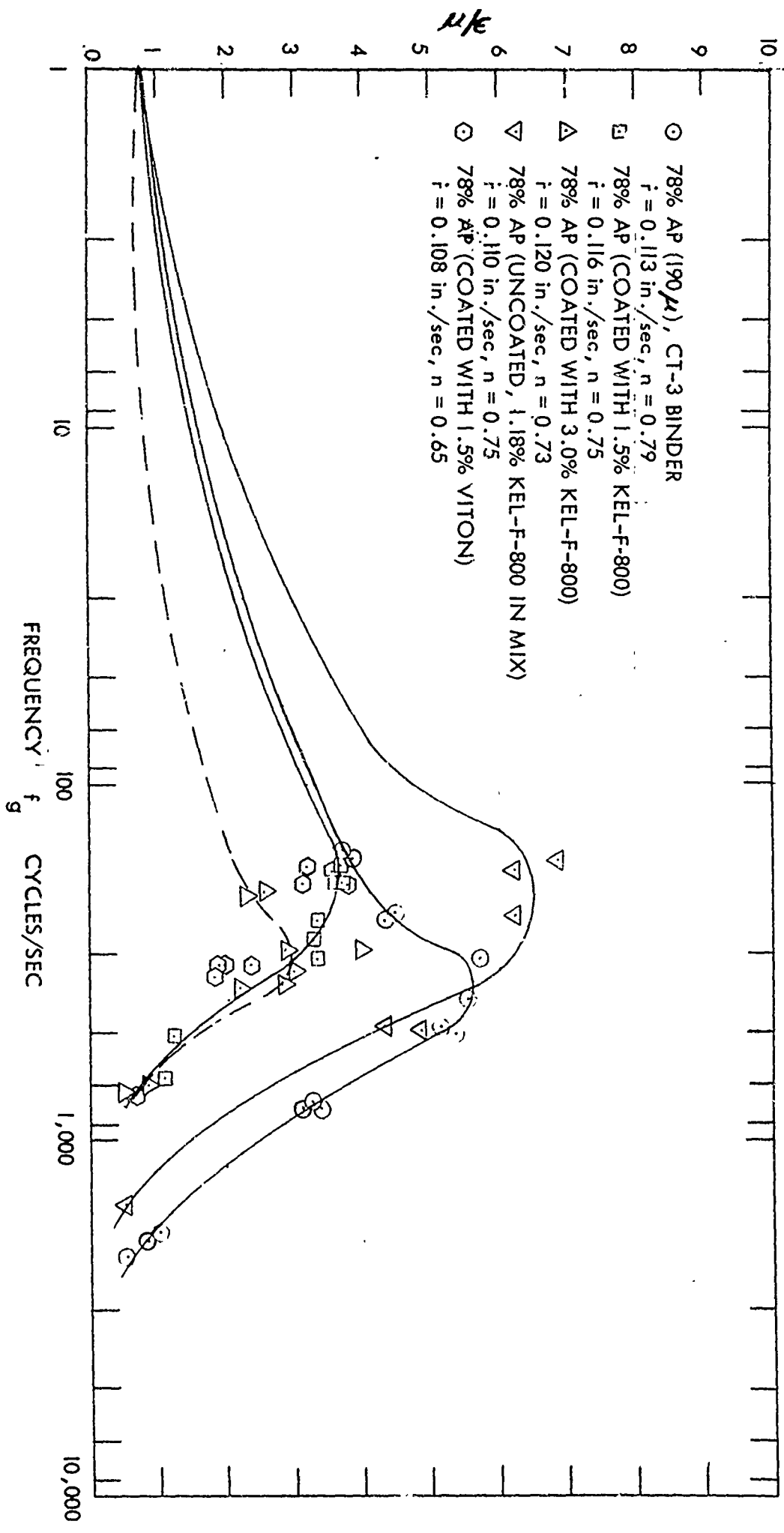


FIGURE 4. EFFECT OF KEL-F AND VITON COATINGS ON ACOUSTICAL RESPONSE

ME

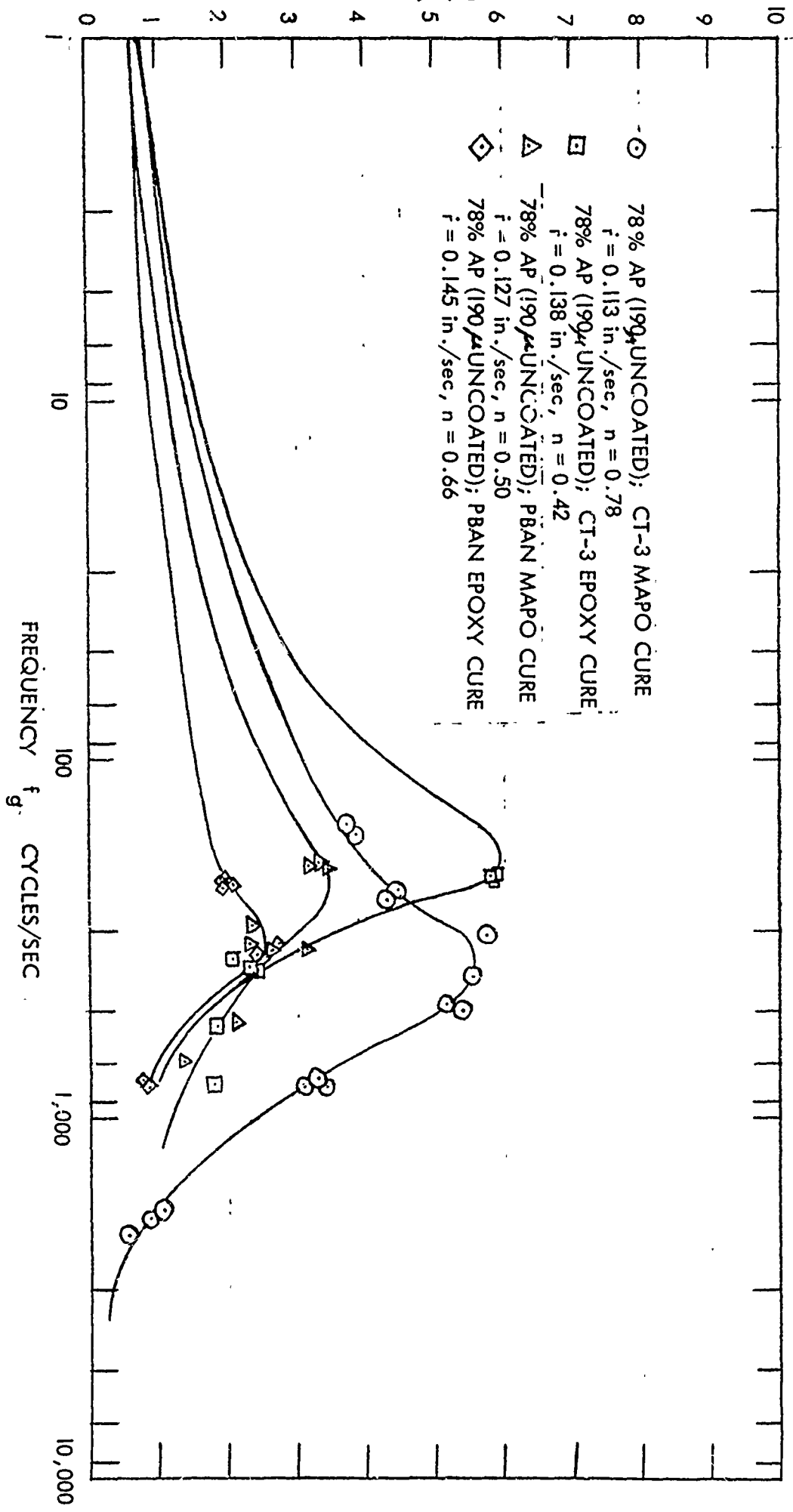


FIGURE 5. EFFECT OF PBAN BINDERS

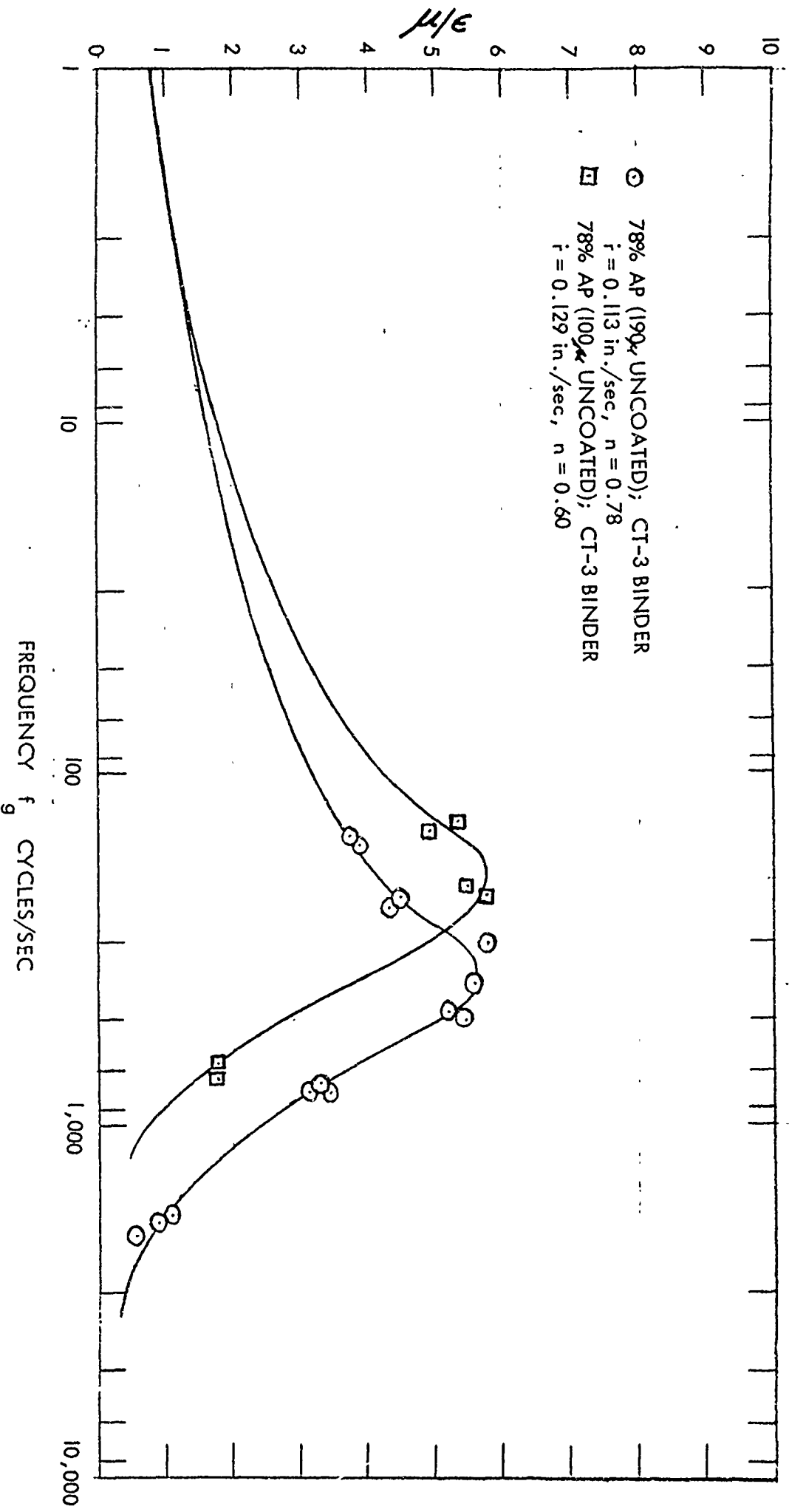


FIGURE 6. EFFECT OF AP PARTICLE SIZE

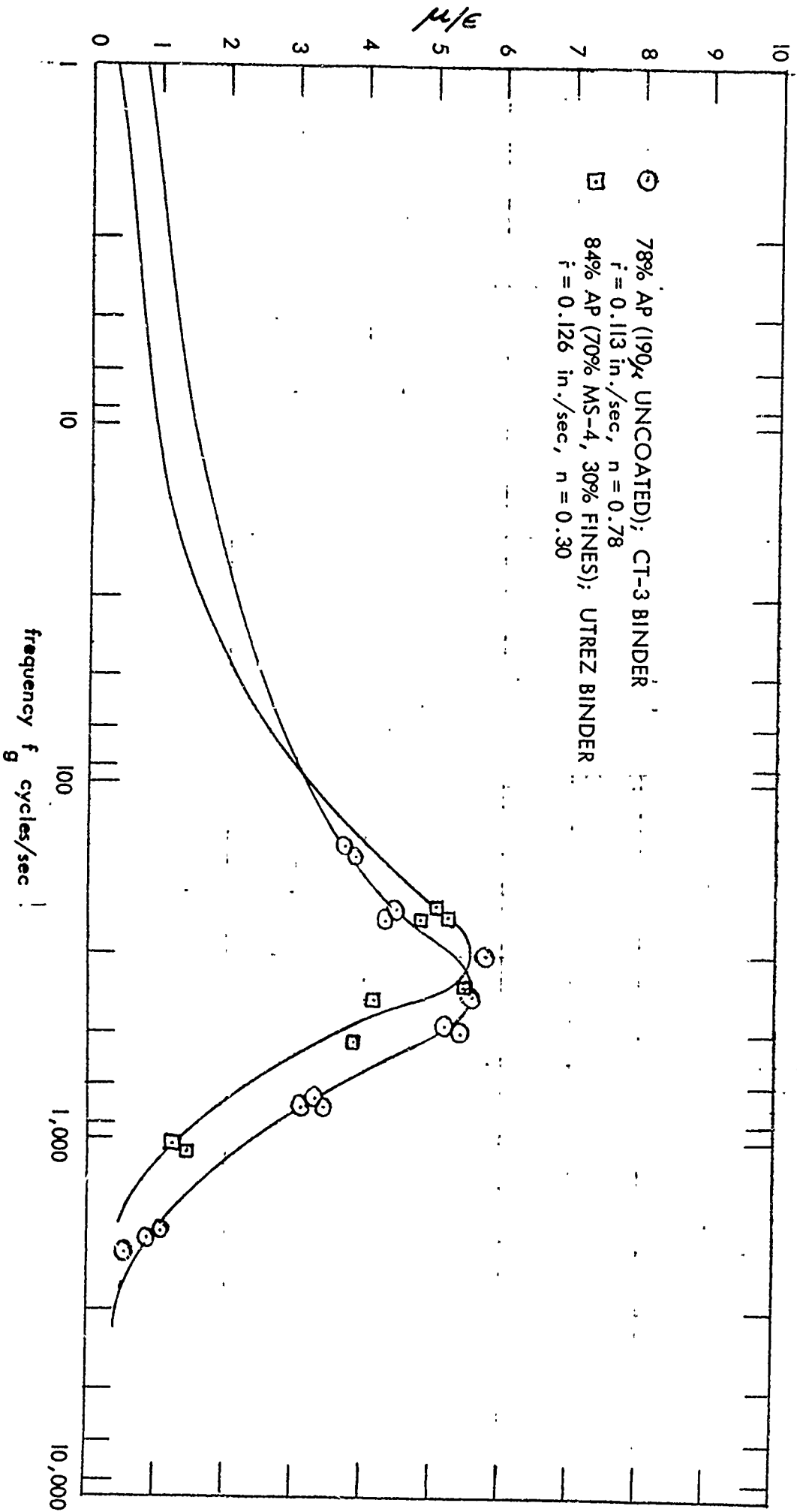


FIGURE 7. UTREZ BINDER FOR MOVIES

APPENDIX B

THEORETICAL ANALYSIS OF SUBSURFACE REACTIONS AND NONLINEAR EFFECTS
USING FINITE DIFFERENCE TECHNIQUES

The equations used to develop the nonlinear algorithm are essentially identical to those being studied for the linear behavior. The principal difference between the two is the manner in which the subsurface reaction term is handled. In the studies using the perturbation technique, this term is neglected, whereas using the finite difference approach this term can be considered.

Using the variables expressed in nondimensional form

$$\theta = T/T_{\infty} \quad (\text{B-1})$$

$$\theta_0 = T_s^{\circ}/T_{\infty} \quad (\text{B-2})$$

$$\tau = t (\dot{r}_0)^2 / \alpha \quad (\text{B-3})$$

$$\zeta = x r_0 / \alpha \quad (\text{B-4})$$

where \dot{r}_0 is the steady-state combustion velocity and $\alpha = k/C_p\rho$, equations B-1 through B-4 become

$$\frac{\partial \theta}{\partial \tau} = \frac{\partial^2 \theta}{\partial \zeta^2} + \frac{\dot{r}}{r_0} \frac{\partial \theta}{\partial \zeta} + \bar{z}_3 e^{-E_3/RT_{\infty}\theta} \quad (\text{B-5})$$

at $\zeta = 0$

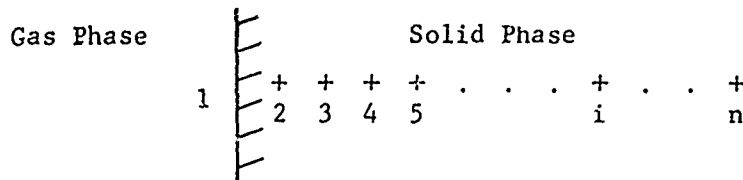
$$-\frac{\partial \theta}{\partial \zeta} = \frac{\eta}{\phi} + \bar{P} \exp \left[-E/RT_{\infty}\theta \right] - \frac{\beta}{\phi} \quad (\text{B-6})$$

$$\zeta \rightarrow \infty \quad \theta \rightarrow 1.0$$

where

$$\bar{P} \equiv \frac{Z P_0}{r_0^2 T_{\infty} C_p}, \quad \bar{z}_3 \equiv \frac{Z_3 \alpha}{T_{\infty} r_0}$$

Exact solution of equations 18, 27, and 28 is difficult because of the nonlinearity of these expressions. In order to circumvent this problem, a finite difference algorithm was developed for digital computer solution. Equation B-5 in continuum form replaced the finite difference approximation as shown by equation B-7 where the mesh points of the difference scheme are represented by i from $i = 1$ at the propellant surface to a point $n\Delta\zeta$ within the solid propellant.



For $i = 2, 3, 4, i, n$

$$\frac{\partial \theta_i}{\partial \tau} = \frac{\theta_{i+1} - 2\theta_i + \theta_{i-1}}{\Delta\zeta^2} + \frac{\dot{r}}{\dot{r}_0} \frac{\theta_{i+1} - \theta_{i-1}}{2\Delta\zeta} + B' e^{-E/RT_\infty} \theta_i \quad (B-7)$$

Writing the boundary condition equation at $\zeta = 0$ in finite difference form results in

$$-\frac{\partial \theta}{\partial \zeta} = \frac{\theta_3 - 4\theta_2 + 3\theta_1}{2\Delta\zeta} = \frac{\eta}{\phi} + \bar{P} e^{-E_2/RT_\infty} - \frac{\beta}{\phi} \left(\frac{\dot{r}}{\dot{r}_c} \right) \quad (B-8)$$

This equation may be differentiated with respect to the time variable, τ , to give

$$\left(\frac{\partial \theta_3}{\partial \tau} - \frac{4\partial \theta_2}{\partial \tau} + 3 \frac{\partial \theta_1}{\partial \tau} \right) / 2\Delta\zeta = \frac{\partial \eta / \phi}{\partial \tau} + \frac{\partial \bar{P}}{\partial \tau} e^{-E_2/RT_\infty} \theta_1 + \bar{P} \frac{E_2}{\theta_1^2 RT_\infty} e^{-E_2/RT_\infty} \theta_1 \frac{\partial \theta_1}{\partial \tau} - \frac{\beta}{\phi} \left(\frac{E_3}{RT_\infty \theta_1^2} \right) \frac{\partial \theta_1}{\partial \tau} \left(\frac{\dot{r}}{\dot{r}_c} \right) \quad (B-9)$$

Rearranging

$$\frac{\partial \theta}{\partial \tau} = \frac{4 \frac{\partial \theta}{\partial \tau} - \frac{\partial \theta}{\partial \tau} + 2 \Delta \zeta \frac{\partial \bar{P}}{\partial \tau} e^{-E_2/RT_{\infty} \theta_1} + \frac{1}{\phi} \frac{\partial \eta}{\partial \tau}}{3 + 2 \Delta \zeta \bar{P} \frac{E_2}{RT_{\infty} \theta_1^2} e^{-E_2/RT_{\infty} \theta_1} + 2 \Delta \zeta \frac{\beta}{\phi} \frac{\dot{r}}{r_0} \frac{E_3}{RT_{\infty} \theta_1^2}} \quad (\text{B-10})$$

Thus, equation B-7 plus the n-1 equations of the form of equation B-4 provides a set of n simultaneous differential equations which can be solved with the aid of a digital computer. From equations 8 and 18 we obtained P , $\partial P/\partial \tau$ and $\partial \eta/\partial \tau$ and the time differential form of equation 9.

In these studies a method of solution has been used which is quite unique in solving the transient diffusion and chemical reaction equations. First, a system of ordinary differential equations is generated from the relevant partial differential equation by discretization in terms of the space variable, and then the sequence of values of the dependent variable at the mesh points are regarded as new dependent variables. This leads to a system of ordinary differential equations (in derivatives with respect to time). This means of solution of boundary value problems was extensively exploited for some time in analogue computer work for solution of such problems as transient conduction of heat in solids. In analogue computer work, the limitation is usually the capacity of the computer. The relatively recent development of digital computer subroutines ("package solvers") "analogue discretization" methods to a competitive means for solving certain types of partial differential equations.

The specific advantages of this approach to solution of boundary problems may be listed as follows:

- A. The programming time is reduced to a minimum as most of the difficult programming has been done in the development of the ordinary differential equations subroutine. Also, the computer running time for the differential equations approach seems to offer an advantage compared to problems involving differencing in both the space and time steps.
- B. Numerical convergence problems, i.e., convergence problems arising in numerical solution of the partial differential equations, are relegated to problems of convergence of solutions of systems of ordinary differential equations. Most subroutines for solution of ordinary differential equations have some means of assurance of numerical convergence of the solution.

- C. Conversion of a boundary value problem into a system of ordinary differential equations provides a means of handling nonlinear difficulties. This point is particularly important because many of our equations involve an exponential Arrhenius term as well as reactant product terms.
- D. The capacity of the differential equation "package solvers" is sufficiently large to allow use of a fairly large number of mesh points in the discretization.

The study of the acoustic response requires that the oscillations occur about the steady state. Hence, the analysis must first predict the steady-state conditions for a given set of combustion parameters and then calculate the transient behavior. To do this, two approaches are possible. One approach is to assume some initial temperature distribution within the solid and let the transient equations relax to the appropriate steady state. The pressure oscillations are then started because the steady state is reacted.

The second approach is to neglect the transient terms and calculate the steady-state conditions by a trial and error process. In this process, the surface temperature is assumed, and the equations are solved using a forward differencing procedure for the temperature deep within the solid. The surface temperature is then adjusted until the desired temperature in the propellant is obtained. The resulting steady-state profile is then used in the transient model and the oscillations initiated immediately.

Of these two possible approaches, the second is preferred for economic reasons. The calculations using the forward difference approach can be done rapidly on the computer in comparison to the transient calculations. Hence, this is the approach used in these studies.

As mentioned in the main body of this report, even this approach did not prove to be economical. The difficulty arose when the steady-state profile was inserted into the transient equations. Even though close convergence was specified, the predicted steady state never matches the exact steady state. When such information is inserted in the transient equations, further relaxation to the true steady state occurs. This relaxation occurs during the initiation of the oscillations and this compounding effect was found to require extremely small ratios of $\Delta\tau/\Delta\xi^2$ to maintain numerical stability. This, in turn, results in extremely long computer running time (i.e., 1/2 to 1 hr) before the steady oscillatory behavior is achieved. Many such calculations would be required to access the effects desired, therefore, these studies were terminated because of the excessive cost.

Unclassified
Security Classification

DOCUMENT CONTROL DATA - R & D		
<i>(Security classification of title, body of abstract and indexing annotation must be entered when the overall report is classified)</i>		
1. ORIGINATING ACTIVITY (Corporate author) United Technology Center Sunnyvale, California		2a. REPORT SECURITY CLASSIFICATION Unclassified
		2b. GROUP
3. REPORT TITLE RESEARCH ON COMBUSTION OF SOLID PROPELLANTS		
4. DESCRIPTIVE NOTES (Type of report and inclusive dates) Final Report, 1 July 1966 thru 31 August 1967		
5. AUTHOR(S) (First name, middle initial, last name) Robert S. Brown and Ray J. Muzzy		
6. REPORT DATE October 1967	7a. TOTAL NO. OF PAGES	7b. NO. OF REFS 30
8a. CONTRACT OR GRANT NO. DA-04-200-AMC-968(X)	9a. ORIGINATOR'S REPORT NUMBER(S) UTC Report 2136 TSR 2	
9. PROJECT NO. c. d.	9b. OTHER REPORT NO(S) (Any other numbers that may be assigned this report)	
10. DISTRIBUTION STATEMENT This document has been approved for public release and sale; its distribution is unlimited.		
11. SUPPLEMENTARY NOTES		12. SPONSORING MILITARY ACTIVITY U.S. Army Ballistic Research Laboratories Aberdeen Proving Ground, Md., 21005
13. ABSTRACT This report describes theoretical and experimental studies to evaluate the effects of surface reactions on the acoustic response function of composite solid propellants. The AP oxidizer crystals were coated and the results showed coatings of Kel F and Vitor reduce the acoustic response, the reduction increasing with increasing coating level. The effect of binder and curing agent on the response function was also investigated. Studies were also made on the effect of pressure on a carboxy-terminated polybutdiene-ammonium perchlorate propellant. The results indicated that over a pressure range from 100 to 500 psia both the maximum value of the acoustic response function and the frequency at which it occurs increased with increasing pressure. On the theoretical side the predictions from the model agreed well with experiment. Progress has been made on the nonlinear analysis also.		

DD FORM 1473
1 NOV 65

REPLACES DD FORM 1473, 1 JAN 64, WHICH IS OBSOLETE FOR ARMY USE.

Unclassified
Security Classification

14. KEY WORDS	LINK A		LINK B		LINK C	
	ROLE	WT	ROLE	WT	ROLE	WT
Combustion Instabilities Acoustic Response Function T-Burners Oxidizers Binders						